AGU PUBLICATIONS

JGR

Journal of Geophysical Research: Earth Surface

RESEARCH ARTICLE

10.1002/2014JF003311

Key Points:
- With a 1-D cross-shore model we study the long-term behavior of tidal flats
- Due to a positive feedback mechanism, a stationary balance can hardly exist
- The flats build out or retreat, depending on the sediment supply and the waves

Correspondence to:
D. C. Maan,
d.c.maan@tudelft.nl

Citation:
Maan, D. C., B. C. van Prooijen, Z. B. Wang, and H. J. De Vriend (2015), Do intertidal flats ever reach equilibrium?, *J. Geophys. Res. Earth Surf*, *120*, doi:10.1002/2014JF003311.

Received 12 AUG 2014
Accepted 3 NOV 2015
Accepted article online 6 NOV 2015

Do intertidal flats ever reach equilibrium?

D. C. Maan[1], B. C. van Prooijen[1], Z. B. Wang[1,2], and H. J. De Vriend[1]

[1]Department of Hydraulic Engineering, Delft University of Technology, Delf, Netherlands, [2]Deltares, Delft, Netherlands

Abstract Various studies have identified a strong relation between the hydrodynamic forces and the equilibrium profile for intertidal flats. A thorough understanding of the interplay between the hydrodynamic forces and the morphology, however, concerns more than the equilibrium state alone. We study the basic processes and feedback mechanisms underlying the long-term behavior of the intertidal system, restricting ourselves to unvegetated intertidal flats that are controlled by cross-shore tidal currents and wind waves and applying a 1-D cross-shore morphodynamic model. The results indicate that by an adjustment of the profile slope and shape, an initial imbalance between deposition and erosion is minimized within a few decades. What follows is a state of long-term seaward progradation or landward retreat of the intertidal flat, in which the cross-shore profile shape is largely maintained and the imbalance between deposition and erosion is not further reduced. These long-term trends can be explained by positive feedbacks from the morphology onto the hydrodynamic forces over the flat: initial accretion (erosion) decreases (increases) the shear stresses over the flat, which induces further accretion (erosion). This implies that a static equilibrium state cannot exist; the flat either builds out or retreats. The modeled behavior is in accordance with observations in the Yangtze Estuary. To treat these unbalanced systems with a one-dimensional numerical model, we propose a moving (Lagrangian) framework in which a stable cross-sectional shape and progradation speed can be derived for growing tidal flats, as a function of the wave climate and the sediment concentration in deeper water.

1. Introduction

Intertidal flats, soft sediment beds located between the mean low water and mean high water spring tide, exist in a variety of environments ranging from tidal basins to estuaries and open coasts [*Flemming*, 2002]. Above mean sea level, intertidal flats generally merge with vegetated salt marshes. Together, salt marshes and intertidal flats form important habitats, where organic material accumulates and numerous types of living organisms gather, feed, rest, breed, and nurse their offspring. The intertidal environment is indispensable to the ecosystem far outside its boundaries and therefore often protected by international legislation, such as the Ramsar Convention for the protection of migratory birds or the European Natura 2000 legislation.

On the other hand, intertidal flats and marshes are highly sensitive to changes in their environmental conditions. Engineering works, aimed to protect the coast or facilitate navigation, as well as anthropogenic climate change and sea level rise, often drastically affect the intertidal area. The Oosterschelde in the Netherlands is an example of a system where an anthropogenic interference (building of a storm surge barrier) resulted in ongoing erosion of the intertidal flats [*Eelkema et al.*, 2013]. In the Yangtze Estuary (China), the intertidal area reduced after the construction of dams in the Yangtze River [*Yang et al.*, 2011]. The Venice Lagoon, on the other hand, is an example of systems where the future of the intertidal flats and salt marshes critically depends on the rate of sea level rise in the next century [*Marani et al.*, 2007].

Erosion of intertidal flats is generally undesirable, as a smaller area or a lower elevation of the flats implies less food or a shorter dry period for wading birds to forage. It also implies a smaller buffer between (migrating) channels and dikes; intertidal flats protect the dikes by providing geotechnical stability and dissipating wave energy [*Dyer*, 1998; *Kirby*, 2000]. In order to support management decisions, a proper understanding of the dynamics of the intertidal system and their response to engineering works and sea level rise is needed.

The functionality of intertidal flats for ecology and coastal defense depends on the shape of their cross-shore profiles [*Kirby*, 2000]. For ecology and safety issues, high and convex upward (decreasing slope toward the top of the tidal flat, henceforth simply called "convex") profiles are generally preferred over low and concave

upward (increasing slope toward the top of the flat, henceforth called "concave") ones for their relatively wide upper intertidal area [*Kirby*, 2000]. Relationships between the cross-shore equilibrium profiles of intertidal flats and the environmental factors (sediment availability, wave climate, and tidal range) have been derived in various studies [*Friedrichs and Aubrey*, 1996; *Roberts et al.*, 2000; *Friedrichs*, 2011], both numerically and analytically. Such a "morphodynamic equilibrium state" is commonly defined by a constant bed level over some characteristic time span. It has been shown that the intertidal cross-shore profile, once in equilibrium with the environment, tends to be convex under the influence of tidal currents, whereas the action of wind waves yields more concave equilibrium profile shapes. For situations in which waves and tidal currents are both present, several authors have suggested that the cross-shore equilibrium profile can be classified according to the "dominance" of waves over tides, i.e., to the relative magnitude of the wave- and tide-induced shear stresses [*Kirby*, 2000; *Roberts et al.*, 2000; *Friedrichs*, 2011].

However, numerous studies show that a stationary morphodynamic equilibrium state is rather exceptional and that coastlines are, in general, in an accretive or erosive state [*Kirby*, 2000; *Pritchard et al.*, 2002; *Van der Wegen*, 2010; *Mariotti and Fagherazzi*, 2010; *Tambroni and Seminara*, 2012]. Numerical studies by *Pritchard et al.* [2002] and *Waeles et al.* [2004] show that under influence of cross-shore tidal currents, intertidal flats prograde or retreat in the long run, whereas the cross-shore profile shape is stable after a few decades of evolution. *Mariotti and Fagherazzi* [2010] and *Tambroni and Seminara* [2012], both accounting for the effects of wind waves and vegetation, show similar trends. Other studies show correlations between the accretive (erosive) state and the convexity (concavity) of the cross-shore profile [*Lee and Mehta*, 1997; *Dyer*, 1998; *Kirby*, 2000, 2002; *Liu et al.*, 2011; *Friedrichs*, 2011], as well as the influence of net sedimentation on the profile slope and the width of the intertidal area [*Pritchard and Hogg*, 2003; *Liu et al.*, 2011; *Friedrichs*, 2011]. Convex and accreting flats have furthermore been linked to tidal dominance and concave and retreating flats to wave dominance [*Mehta et al.*, 1996; *Kirby*, 2000; *Friedrichs*, 2011], although *Pritchard et al.* [2002] showed that tidal asymmetry can significantly change the effect of tides and that ebb dominance can cause the tidal flat to retreat with a convex profile shape.

Subsequent studies sought for the criteria for which intertidal flats prograde or retreat and for which an equilibrium state develops. *Waeles et al.* [2004] incorporated the effect of wind waves in their 1-D cross-shore model and found that the possibility of an equilibrium state depends on the typical wave regime. *Mariotti and Fagherazzi* [2010] showed that the state (progradation or retreat) furthermore depends on the sediment supply and that the presence of vegetation influences the rate of progradation or retreat. In the same study, the evolution of the marsh boundary and adjacent flat was determined for different scenarios of sea level rise. Their results show that sea level rise (in time) is an important factor, which can determine whether an intertidal flat will prograde or retreat.

Additional relevant studies on the intertidal morphodynamic equilibrium were carried out within 0-D frameworks [*Fagherazzi et al.*, 2006, 2007; *Marani et al.*, 2007; *De Swart and Zimmerman*, 2009; *Marani et al.*, 2010], i.e., based on the assumption of a homogeneous bed level (platform). This approach is based on observations of characteristic intertidal landscapes in which large tidal platforms lie within specific ranges of elevation (separated by much steeper transition zones). Results of these studies suggest that wave-dominated intertidal platforms migrate to stable equilibrium elevations [*Fagherazzi et al.*, 2006; *Marani et al.*, 2007; *De Swart and Zimmerman*, 2009; *Marani et al.*, 2010] and that the presence of vegetation and biomorphodynamic feedbacks can further intensify the discrepancy between different stable elevations [*Fagherazzi et al.*, 2006, 2007; *Marani et al.*, 2007, 2010].

The present study is motivated by the wish to predict the consequences of engineering works for the status of the intertidal flats in the Yangtze Estuary. The mudflats around the mouth of the Yangtze River are characterized by the exposure to wind waves and the large supply of fine sediment from the Yangtze River [*Yang et al.*, 2008]. Studies show that both wind wave- and tide-induced forces play a significant role in the morphodynamics of these flats [*Yang et al.*, 2001, 2008]. In the period between 1982 and 1990, the intertidal flats prograded with a smooth and convex shape (see Figure 1), presumably as a consequence of the abundant sediment supply from the river. In the last few decades, the construction of dams in the river basin has resulted in a strong reduction of the sediment supply. Subsequently, the progradation of the tidal flats has stopped and the profiles have become more and more concave [*Yang et al.*, 2011]. Yet the future of the intertidal flats in the Yangtze Estuary remains uncertain: will the flats further prograde after a change in shape, will a stationary balance be established, or is the change in shape an early indication for (long-term) erosion?

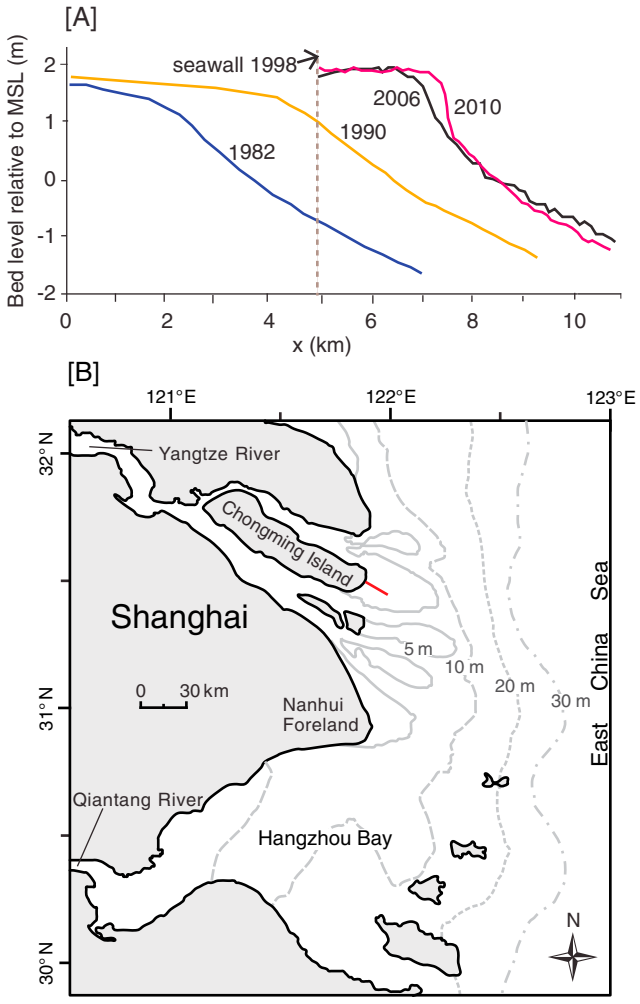

Figure 1. (a) Observed cross-shore profiles near mean sea level at Eastern Chongming Island, modified from *Yang et al.* [2011]. Indicated distances are relative to the 1980 seawall (km). The figure shows similar convex up cross-sections in 1982 and 1990 in combination with a horizontal progradation of the coastline. The profiles in 2006 and 2010 show concave lines. (b) Map of the Yangtze River Delta; the red line indicates the transect in Figure 1a.

In this study we aim to determine the influence of the sediment supply and the wave climate on the state (prograding, retreating, or in equilibrium) of intertidal flats that are dominated by cross-shore processes (cross-shore tidal currents and wind waves) and to describe the morphodynamic feedback mechanisms that underlie their long-term trends. We explicitly focus on the response of the intertidal system to constant environmental conditions. Understanding the behavior of such a simplified system is a first step in predicting the consequences of engineering works and of sea level rise for the status of intertidal flats. The role of biological processes and salt marshes in the long-term biomorphodynamic evolution of intertidal flats are discussed by several recent studies [*van de Koppel et al.*, 2005; *Marani et al.*, 2007, 2010; *Mariotti and Fagherazzi*, 2010], but we focus on the interactions between the hydrodynamics and the cross-shore morphology on a bare intertidal flat.

The behavior of the intertidal system is investigated by analyzing the evolution of the bathymetry and the patterns of suspended sediment concentration and shear stresses, as well as the horizontal sediment fluxes, over developing tidal flats with a 1-D cross-shore morphodynamic model (section 2). In section 3, the model is expressed in a moving reference frame, a way to derive the stable profile shapes and migration velocities as a function of the wave climate and sediment supply from deeper water. The stable profile shapes and migration velocities are derived for two different combinations of hydrodynamic forcing: (1) tidal currents only and (2) tidal currents plus wind waves. Our results are used to interpret the development of the flats in the Yangtze Estuary in section 4. Although the tidal flats in the Yangtze Estuary are likely also influenced by long-shore

currents, especially on the deeper part of the intertidal area [*Le Hir et al.*, 2000], we believe that our results provide an explanation for the first-order processes that underlie the migration of these flats in the cross-shore direction. Conclusions are drawn in section 5.

2. Eulerian Framework

2.1. Model Description

Process-based numerical models provide the framework to study the basic processes underlying the intertidal flat evolution. We developed a 1-D cross-shore model that computes cross-shore tidal flow and the growth (shoaling) and decay (dissipation and breaking) of incoming wind waves over a tidal flat, the associated tide- and wave-induced shear stresses, the sediment transport, and the induced morphological changes. By using a cross-shore model, we neglect the effect of the long-shore current and long-shore sediment transport on the cross-shore profile and any other interaction with the long-shore dimension. The study is therefore applicable for wide, gently sloping tidal flats, normally found at locations with a large supply of fine sediment [*Flemming*, 2002]. The model is however more comprehensive than the 1-D cross-shore models used by *Roberts et al.* [2000] and *Pritchard et al.* [2002], because it includes a more detailed description for the effects of wind waves on the bed shear stress. Furthermore, we do not neglect the dispersion term in the sediment transport equation (equation (4)). Actually, our model is quite similar to the one used by *Waeles et al.* [2004], although we do not include the effects of nonlinear current and wave interactions and the presence of biota on the bed shear stress.

The model is forced by a constant external sediment concentration at the boundary, which is assumed to be independent of the intertidal flat morphodynamics and the gain or loss of sediment over the tidal flat. This boundary can be formed by a tidal channel, for instance, or the mouth of a river, in which the sediment concentration is largely determined by other (larger-scale) processes.

The water depth and cross-shore tidal currents are evaluated in time by the conservation equations for mass and momentum, respectively,

$$\frac{\partial h}{\partial t} + \frac{\partial uh}{\partial x} = 0, \tag{1}$$

$$\frac{\partial u}{\partial t} + u\frac{\partial u}{\partial x} = -g\frac{\partial \zeta}{\partial x} - \frac{\tau_{bc}}{\rho_w h} \tag{2}$$

where h is the water depth, u is the cross-shore flow velocity, ζ is the water level, g is the acceleration due to gravity, ρ_w is the density of water, and τ_{bc} represents the bed shear stress (i.e., bed-induced friction on the flow), given by the quadratic drag law:

$$\tau_{bc} = \rho_w C_d u^2. \tag{3}$$

in which C_d is a constant drag coefficient (Table 1), see *Soulsby* [1997]. Hence, the effect of wind shear stress on the depth-averaged flow is not calculated. Wind waves are, however, included by making an assumption for the height of the incoming wind waves at the model boundary (see below).

The sediment concentration is described by the advection-dispersion equation:

$$\frac{\partial ch}{\partial t} + \frac{\partial uch}{\partial x} - \frac{\partial}{\partial x}\left(Kh\frac{\partial c}{\partial x}\right) = E - D, \tag{4}$$

where c is the suspended sediment concentration, K is the dispersion coefficient, and E and D are the vertical erosion and deposition fluxes, respectively, (see equations (13) and (14)). For the computation of the flow and sediment transport we apply a minimum depth of 10 cm for the flooding-drying procedure (i.e., at smaller depths the flow velocity and the sediment transport rates are taken equal to zero).

The wave height at the model boundary is set at each time step by a random draw from the Rayleigh distribution around a constant mean value (Table 1). The model calculates the corresponding wave height at each grid cell, taking into account wave shoaling and dissipation due to bed friction, by the continuity equation for the wave energy flux [*Christoffersen and Jonsson*, 1985]:

$$\frac{dE_f}{dx} = \frac{d}{dx}\left(\frac{1}{8}\rho_w g H^2 c_g\right) = -D_w, \tag{5}$$

Table 1. Settings for Model Parameters

Parameter	Value	Description
w_s	$0.2 \cdot 10^{-3}$	Settling velocity (m s^{-1})
m_e	$5 \cdot 10^{-5}$	Erosion coefficient (kg m^{-2} s^{-1})
τ_{cr}	0.1	Critical shear stress for erosion (N m^{-2})
K	100	Dispersion coefficient (m^2 s^{-1})
ρ_{dry}	900	Dry bed density (kg m^{-3})
d_{50}	30	Mean sediment diameter (μm)
T	2	Wave period (s)
H_0	0.2	Average wave height at the model boundary (m)
C_d	0.003	Drag coefficient [*Soulsby*, 1997]
$[T_{M2}, H_{M2}]$	[12.4167, 1.356]	M2 tidal constituent [period(h),amplitude(m)]
$[T_{S2}, H_{M2}]$	[12, 0.6440]	S2 tidal constituent [period(h),amplitude(m)]
dt	40	Time step (s)
dx	200	Grid size (m)

in which E_f is the wave energy, H the wave height, c_g the group velocity, and D_w the energy dissipation. c_g is given by linear wave theory

$$c_g = \frac{c_w}{2}\left(1 + \frac{2\kappa h}{\sinh(2\kappa h)}\right), \tag{6}$$

in which c_w is the phase velocity:

$$c_w = \sqrt{\frac{g}{\kappa}\tanh(\kappa h)}. \tag{7}$$

The wave number κ is related to the water depth and the wave period (Table 1) via the dispersion relation according to linear wave theory (computed via a numerical iteration algorithm based on Newton's method).

The energy dissipation in the wave boundary layer can be related to the amplitude of the wave orbital velocity, U_δ, and the "energy loss factor" f_e [*Justesen*, 1988; *Fredsoe and Deigaard*, 1992]:

$$D_w = \frac{2}{3\pi}\rho_w f_e U_\delta^3. \tag{8}$$

U_δ is given by [*Van Rijn*, 1993]

$$U_\delta = \frac{\pi H}{T\sinh(\kappa h)}, \tag{9}$$

The energy loss factor can be approximated by the wave friction factor [*Justesen*, 1988; *Fredsoe and Deigaard*, 1992], which is calculated by [*Swart*, 1976]

$$f_w = \min\left[\exp\left(-6 + 5.2 \cdot \left(\frac{A_\delta}{2.5 \cdot d_{50}}\right)^{-0.19}\right), 0.3\right], \tag{10}$$

in which A_δ is the amplitude of the wave orbital excursion,

$$A_\delta = \frac{U_\delta}{\omega}, \tag{11}$$

with $\omega = 2\pi/T$ the wave angular velocity.

Furthermore, the change in wave height due to wave breaking in the surf zone is taken into account by limiting the wave height to a fraction f_r of the water depth, i.e.,

$$H = \min\left[H, f_r d\right] \tag{12}$$

This criterion is applied after the derivation of the wave height by equation (5). Our results are produced with $f_r = 0.7$, but the model has been run for different fractions as well, ranging from 0.5 to 0.8. Although the distribution and the peak value of the wave energy on the flat are altered significantly by this parameter, this is not relevant for the concepts that are presented in this paper.

The erosion and deposition fluxes in equation (4) are computed by [*Ariathurai*, 1974; *Winterwerp and Van Kesteren*, 2004]

$$E = \max\left[m_e\left(\frac{\tau_b'}{\tau_{\mathrm{cr}}} - 1\right), 0\right] \tag{13}$$

and

$$D = c \cdot w_s, \tag{14}$$

where m_e is the erosion rate coefficient, τ_b' the total skin friction acting on the grains (i.e., that part of the total bed shear stress that directly acts on the sediment particles [*Fredsoe and Deigaard*, 1992], see equation (15)), τ_{cr} the critical bed shear stress for erosion, and w_s the settling velocity. This description, which does not include a critical bed shear stress for deposition, implies that erosion and deposition occur simultaneously when the shear stress exceeds its critical value for erosion [*Winterwerp and Van Kesteren*, 2004]. Bed load transport is not taken into account; we focus on intertidal flats that are composed of fine sediments.

The total skin friction consists of a wave- and a tide-induced part, which are assumed to be additive (neglecting nonlinearities due to wave-current interactions, see *Soulsby and Clarke* [2005]):

$$\tau_b' = \tau_{\mathrm{bc}}' + \tau_{\mathrm{bw}}'. \tag{15}$$

The tide-induced skin friction is derived from the tidal flow velocity [*Van Rijn*, 1993]:

$$\tau_{\mathrm{bc}}' = \frac{1}{8}\rho_w f_c u^2, \tag{16}$$

with friction factor

$$f_c = 0.24\left(\log\left(\frac{12 \cdot h}{2.5 \cdot d_{50}}\right)\right)^{-2}, \tag{17}$$

where d_{50} is the median sediment diameter. The wave-induced skin friction is calculated by [*Van Rijn*, 1993]

$$\tau_{\mathrm{bw}}' = \frac{1}{4}\rho_w f_w U_\delta^2, \tag{18}$$

which is related to the wave height via equation (9). The model does not account for any extra shear stress due to wave breaking induced turbulence.

After calculating the erosion and deposition fluxes, bed level changes are computed from

$$\frac{\mathrm{d}\eta}{\mathrm{d}t} = \frac{1}{\rho_{\mathrm{dry}}}(D - E), \tag{19}$$

in which ρ_{dry} is the dry bed density (Table 1) and D and E the deposition and erosion fluxes. ρ_{dry} is assumed to be constant in time; i.e., the difference in compaction between freshly deposited mud and the older bed is neglected.

For some simulations, a so called "morphological factor" M is used to speed up the calculation process [*Lesser et al.*, *Roelvink*, 2006]. Bed level changes over a period of M spring-neap cycles are then derived by calculating the bed level changes over one spring-neap cycle and multiplying, at each hydrodynamic time step, the bed level changes by M. This method can only be applied when the bed level changes within the considered time period (M times the spring-neap period) are so small that they do not significantly affect the hydrodynamics.

Table 2. Simulation Codes With Boundary Conditions and Parameter Values

Code	c_0 (kg m^{-3})	Waves (m)	K (m^2 s^{-1})	w_s (m s^{-1})	M
*E*1	0	no	100	$0.2 \cdot 10^{-3}$	50
*E*2	0.15	no	100	$0.2 \cdot 10^{-3}$	10
*E*3	0.05	0.2	100	$0.2 \cdot 10^{-3}$	20
*E*4	0.3	0.2	100	$0.2 \cdot 10^{-3}$	20
*E*5	$5 \cdot 10^{-4}$	0.2	1	$0.2 \cdot 10^{-3}$	20
*Lg*1	0.01	no	100	$0.2 \cdot 10^{-3}$	5
*Lg*2	0.1	no	100	$0.2 \cdot 10^{-3}$	5
*Lg*3	0.2	no	100	$0.2 \cdot 10^{-3}$	5
*Lg*4	0.3	no	100	$0.2 \cdot 10^{-3}$	5
*Lg*5	0.1	0.2	100	$0.2 \cdot 10^{-3}$	10
*Lg*6	0.2	0.2	100	$0.2 \cdot 10^{-3}$	10
*Lg*7	0.3	0.2	100	$0.2 \cdot 10^{-3}$	10
*Lg*8	0.4	0.2	100	$0.2 \cdot 10^{-3}$	5
*Lg*9	0.1	0.2	1	$0.2 \cdot 10^{-3}$	1
*Lg*10	0.2	0.2	1	$0.2 \cdot 10^{-3}$	1
*Lg*11	0.3	0.2	1	$0.2 \cdot 10^{-3}$	1
*Lg*12	0.4	0.2	1	$0.2 \cdot 10^{-3}$	1
*Lg*13	0.1	0.2	100	$0.5 \cdot 10^{-3}$	1
*Lg*14	0.2	0.2	100	$0.5 \cdot 10^{-3}$	1
*Lg*15	0.3	0.2	100	$0.5 \cdot 10^{-3}$	1
*Lg*16	0.4	0.2	100	$0.5 \cdot 10^{-3}$	1

The effect of this factor was therefore always verified at different stages of the simulation by running a similar model with smaller factors in parallel during certain time intervals. The values for the applied factors are indicated in Table 2.

The shallow-water equations were implemented on a staggered grid following the description by *Stelling and Duinmeijer* [2003], with the only difference that the flow velocity in the water level points is approximated by a midpoint scheme (taking the average of the two faces; this gives a more accurate approximation of the flow velocities near the tidal front, compared with an upwind scheme). The continuity equation for the wave energy flux (given by equations (5) and (8)) is discretisized by a simple first-order forward difference scheme.

2.2. Parameters and Boundary Conditions

To run the model, several physical and numerical parameters have to be set (see Table 1 for an overview). One of the most uncertain parameters is the horizontal dispersion coefficient K. Following *Ter Brake and Schuttelaars* [2010] and *van Prooijen and Wang* [2013], we assume $K = 100$ m^2 s^{-1}, in order to empirically represent a number of mixing processes that cannot be resolved in a 1-D framework. Note that mixing does occur not only due to (small-scale) turbulence but also, for instance, by larger-scale flow patterns and circulations that result from irregularities in the 2-D bathymetry and geometry [*Fischer*, 1976; *Zimmerman*, 1976; *Geyer and Signell*, 1992]. As we cannot include any of these underlying processes in a 1-D model, we account for their mixing effect by a dispersion term in equation (4). The sensitivity to this parameter has been tested by a comparison with results for $K = 1$ m^2 s^{-1} (section 2.3.5).

Since the evolution of the Yangtze tidal flats has our particular interest, many of the other parameters were chosen to correspond with the conditions in the Yangtze Estuary [*Hu et al.*, 2009; *Chu et al.*, 2010; *Shi et al.*, 2012]. The sensitivity of the results to a limited amount of parameter variations has been tested (section 3.3). Although the values of the model parameters influence the morphodynamic evolution for a given set of boundary conditions, they were found to have less effect on the different types of solutions that can be found by varying the boundary conditions; our qualitative results are therefore expected to be valid for a rather wide range of parameter values.

Also boundary conditions have to be imposed. At the seaward boundary, the water level is described by a symmetric spring-neap tidal cycle:

$$\zeta(t) = H_{M2} \cdot \cos\left(\frac{2\pi}{T_{M2}}t\right) + H_{S2} \cdot \cos\left(\frac{2\pi}{T_{S2}}t\right), \tag{20}$$

in which H_{M2} and T_{M2} and H_{S2} and T_{S2} are the amplitude and period of the $M2$ and $S2$ harmonic constituents, respectively (Table 1). The effect of an asymmetric tidal variation at the boundary on the equilibrium profile shapes and the long-term trends is captured by *Pritchard et al.* [2002]. They found that a flood-dominant regime enhances the tendency of the flat to accumulate sediment and prograde, while an ebb-dominant regime leads to export of sediment and a retreating flat. Both types of asymmetries furthermore resulted in steeper cross-shore profiles compared with a symmetric tidal variation. In the current study we describe the dependencies of the state of the flat (stationary, prograding, or retreating) on the sediment availability and the wave climate in case of a symmetric tidal variation. However, the effect of the superharmonic $M4$ tide for the situation in the Yangtze Estuary (where the ratio between the $M4$ and the $M2$ tide is smaller than 0.2 [*Chu et al.*, 2010]) was investigated. The inclusion of the $M4$ tide, tested for different phase lags, did not significantly affect the results that are presented in this paper.

At the same boundary, a constant value is imposed for the sediment concentration (i.e., tidal variation in the sediment concentration at the boundary is not taken into account) and for the mean wave height (Table 1). At the landward boundary the flow velocity is set equal to zero, representing a closed boundary (sea wall). The possibility of reflection of wind waves at the closed boundary is neglected.

The initial profiles are straight lines. The obtained steady profile shapes are independent of the initial shape and slope, but it is important that the initial profile is chosen not too high and steep (because the top of the intertidal range cannot easily erode once it is established).

2.3. Results

2.3.1. Tides Only—Stationary

The response of intertidal flats to a constant sediment concentration at their boundary is investigated for two different settings of the hydrodynamic forcing: (1) tidal currents only and (2) tidal currents plus wind waves. Each simulation is given a code as indicated in the caption of the figures, and an overview of the corresponding boundary conditions is given in Table 2. For reasons of convenience, the time intervals and time spans indicated in the captions are rounded values. The exact time step does always correspond with a whole number of tidal periods.

We first consider the simulations without wind waves. Figure 2 shows a simulation for a sediment concentration of 0 kg m^{-3} at the boundary. Starting from a linear profile, the adjustment of the profile slope and shape is rapid in the first decades. After approximately 200 years, the flat is stable. At this stage, the instantaneous shear stresses on the profiles do not exceed the critical value for erosion ($\tau_{cr} = 0.1$ N m^{-2}, Figure 3), so that there is no sediment transport.

2.3.2. Tides Only—Progradation

Also for a boundary concentration of 0.15 kg m^{-3}, the adjustment of the profile slope and shape is rapid in the first decades (Figure 4). In this case, the intertidal flat evolves into a state of steady progradation. Roughly, three phases can be distinguished in this simulation, indicated by $P1$ – $P3$ in Figure 4:

1. Within the first few decades, the slope and shape adjust from an initial profile to a relatively stable shape. Hence, the initial erosion of the lower flat, which steepens the profile before accretion, starts to dominate everywhere on the flat.
2. A longer period follows in which accretion is mainly translated into a horizontal progradation.
3. The shape changes significantly when the intertidal area (above mean sea level (msl) −2 m in the figure) reaches the model boundary. This phase is physically irrelevant, since long-shore processes (which we neglect) will be dominant if the intertidal flat approaches the model boundary (note that the boundary represents the conditions in a tidal channel).

The tide-averaged gross erosion and deposition fluxes (Figure 5a) have a maximum at the boundary and decrease toward the top of the flat. The sedimentation rates are much smaller than the gross erosion and deposition fluxes (compare Figures 5a and 5b). An exact balance is, however, not reached: the tide-averaged

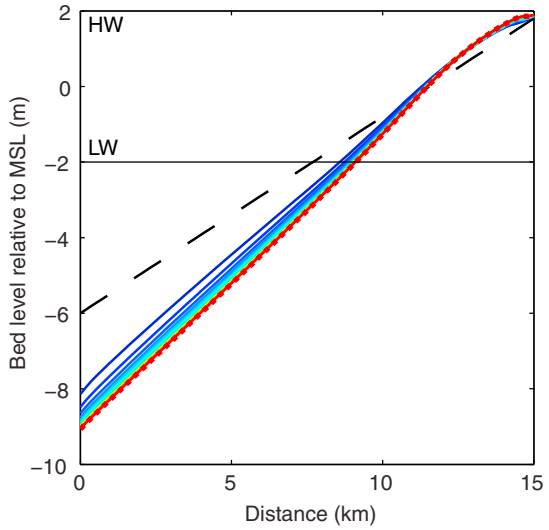

Figure 2. Evolution from an initial bathymetry (from the dashed black line, via the solid colored lines, to the dotted red line), forced with tidal currents only and without suspended sediment at the boundary ($c_0 = 0$ kg m^{-3}) , plotted for a total time span of 240 years and time intervals of 40 years (simulation *E*1, see Table 2).

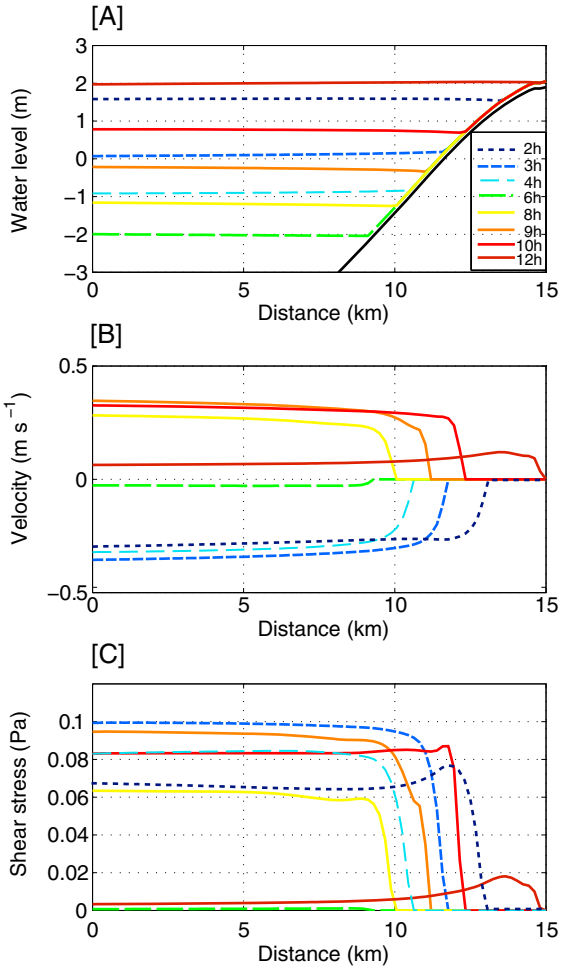

Figure 3. (a) Water levels, (b) flow velocities, and (c) shear stresses at different moments during a tidal cycle (at spring tide) on the equilibrium profile after 240 years of morphodynamic evolution under influence of tidal currents only and $c_0 = 0$ kg m^{-3}, i.e., on the dotted red profile in Figure 2 (simulation *E*1).

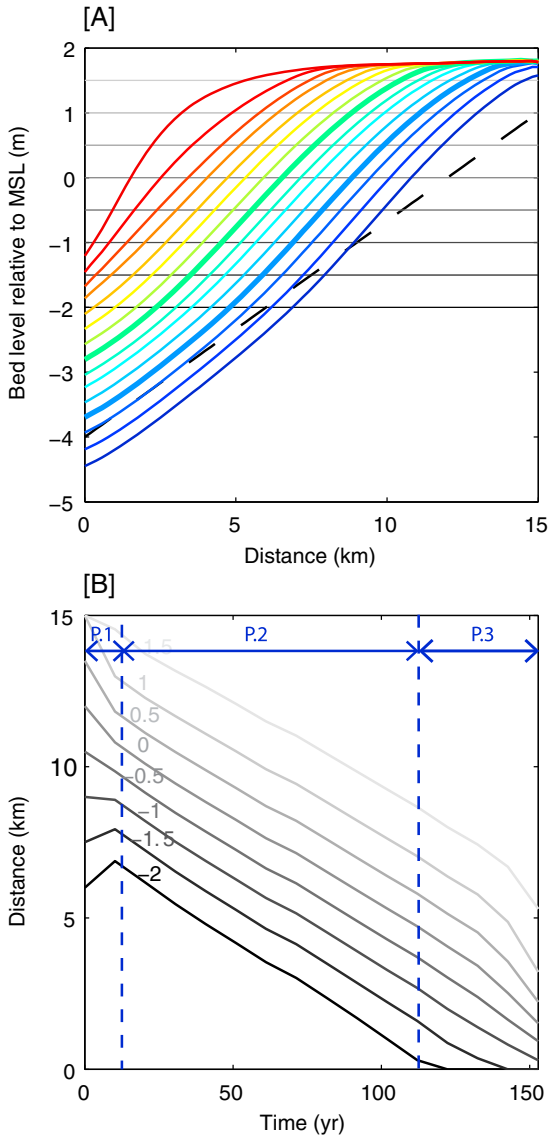

Figure 4. (a) Evolution from an initial bathymetry (from the dashed black line, via the colored lines, to the red line), in case of tides only and $c_0 = 0.15$ kg m^{-3} (simulation *E2*). The total time span is 160 years with plotting time steps of 10 years. The gray horizontal lines refer to the bed levels of the lines in Figure 4b. (b) Distance toward the open boundary against time for different bed levels in the intertidal zone. Straight lines indicate that the progradation speed is constant in time (constant celerity). Parallel lines indicate a pure horizontal shift (uniform celerity). Convergence or divergence of the lines indicate shape changes. At a relative short time scale, the flat evolves into a prograding system in which the shape is largely maintained and the progradation speed is constant in time (phase 2).

sedimentation rates remain of the same order of magnitude throughout the steady progradation stage. Horizontally, advection is the dominant process over most of the flat (Figure 5c). Both the advection and dispersion fluxes induce a landward sediment transport, i.e., in the direction down the tide-averaged concentration gradient (compare Figures 5a and 5b; note that the deposition in Figure 5a is directly proportional to the concentration, equation (14)).

2.3.3. Tides and Wind Waves—Retreat

Subsequently, we consider the simulations with wind waves. For 0.05 kg m^{-3} at the open boundary, a long-term erosive state develops (Figure 6). The uppermost part of the tidal range fills up in the very early stage of the evolution (within the first decades), so that a bank is formed at the top. A stationary equilibrium state is only reached after a large part of the intertidal area is eroded away (see Figure 6). During the erosive stage, the cross-shore shape of the profile (excluding the top) is largely maintained, as can be seen from the

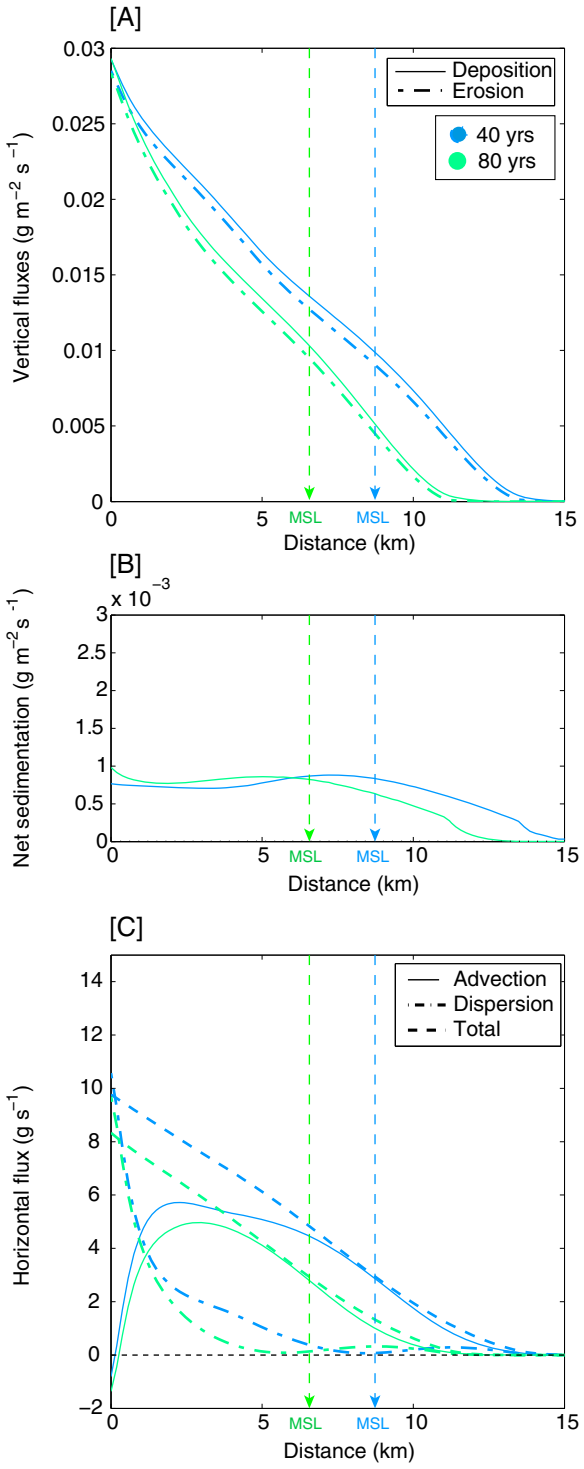

Figure 5. Tide-averaged sediment fluxes over the developing flat of Figure 4 after 40 years (dark blue) and 80 years (light green) of evolution, i.e., corresponding with the thick dark blue and light green profiles in Figure 4a, respectively (simulation *E*2). (a) Deposition and erosion fluxes. (b) Net sedimentation. (c) Horizontal advection and dispersion fluxes. Landward is defined positive.

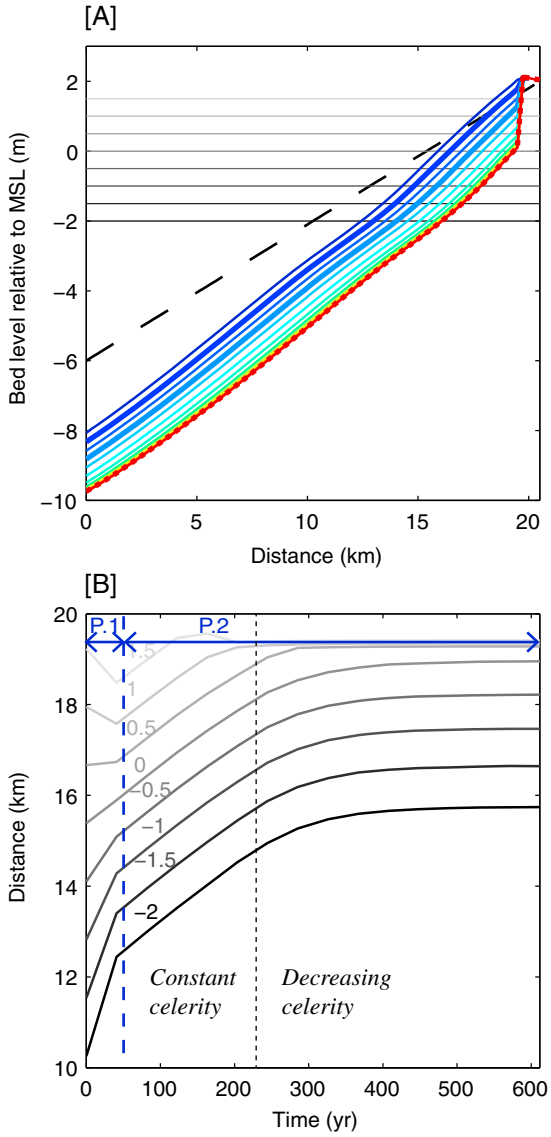

Figure 6. (a) Evolution from an initial bathymetry (from dashed black, via solid colored, to dotted red) in case of tides and wind waves (0.2 m) and a suspended sediment concentration at the boundary of 0.05 kg m^{-3} (simulation *E*3). The total time span is 600 years with steps of 40 years. In the last 200 years the bathymetry (red line) did not change any longer. (b) Distance toward the open boundary against time for different bed levels in the intertidal zone. Straight lines indicate a constant celerity. Parallel lines indicate an uniform celerity. Convergence or divergence of the lines indicate shape changes. The intertidal flat below the top part shifts horizontally with a stable cross-shore profile.

parallel lines in Figure 6b. The maintenance in cross-shore shape implies that the whole intertidal flat, except for the top, retreats landward (henceforth, we will therefore refer to this state as "retreating," despite the fixed position of the bank).

Figures 7a and 7c indicate that peaks in the instantaneous wave-induced shear stresses occur close to the tidal front, i.e., in very shallow waters. The tide-averaged gross erosion and deposition fluxes have a wave-induced maximum on the intertidal flat, and the peaks shift landward with the migration of the flat (Figure 8a). Note that the maximum of the tide-averaged fluxes is determined by a combination of (1) the magnitude of the shear stresses during the period in which a section is underwater (which increases with increasing bed elevation due to maximum wave-induced shear stress in very shallow waters, see Figure 7) and (2) the period in which the section is underwater (which decreases with increasing bed elevation). The net sedimentation rates are small but do not significantly decrease during the state of gradual retreat (Figure 8b). Horizontally, the gross landward advection and dispersion terms are of similar magnitude but of opposite direction (Figure 8c).

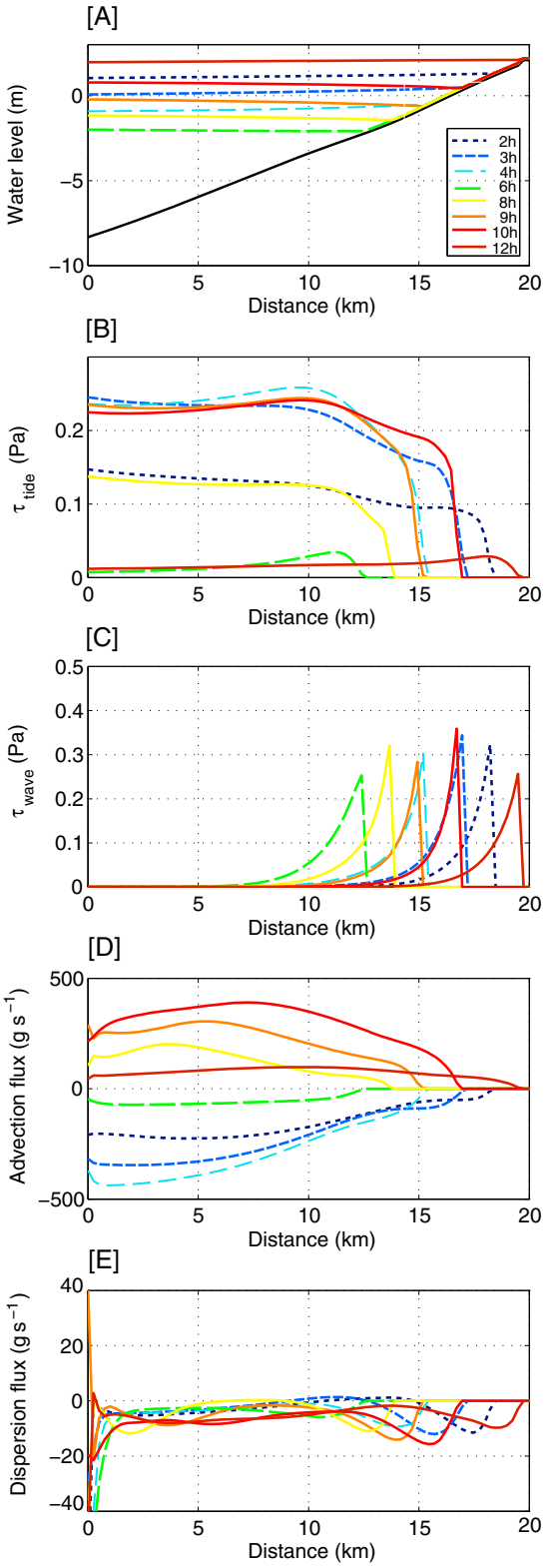

Figure 7. (a) Water levels, (b and c) tide- and wave-induced shear stresses, and (d and e) horizontal fluxes at different moments within a tidal cycle (during spring tide) on a profile that is obtained after 80 years of morphodynamic evolution under influence of tidal currents and wind waves and $c_0 = 0.05$ kg m^{-3}, i.e., on the thick dark blue profile in Figure 6a (simulation *E*3). In order to better compare the wave-induced force at different elevations, a constant wave height at the boundary has been chosen ($H_0 = 0.2$ m), instead of the random draw from the Rayleigh distribution that has been used for the morphodynamic calculations.

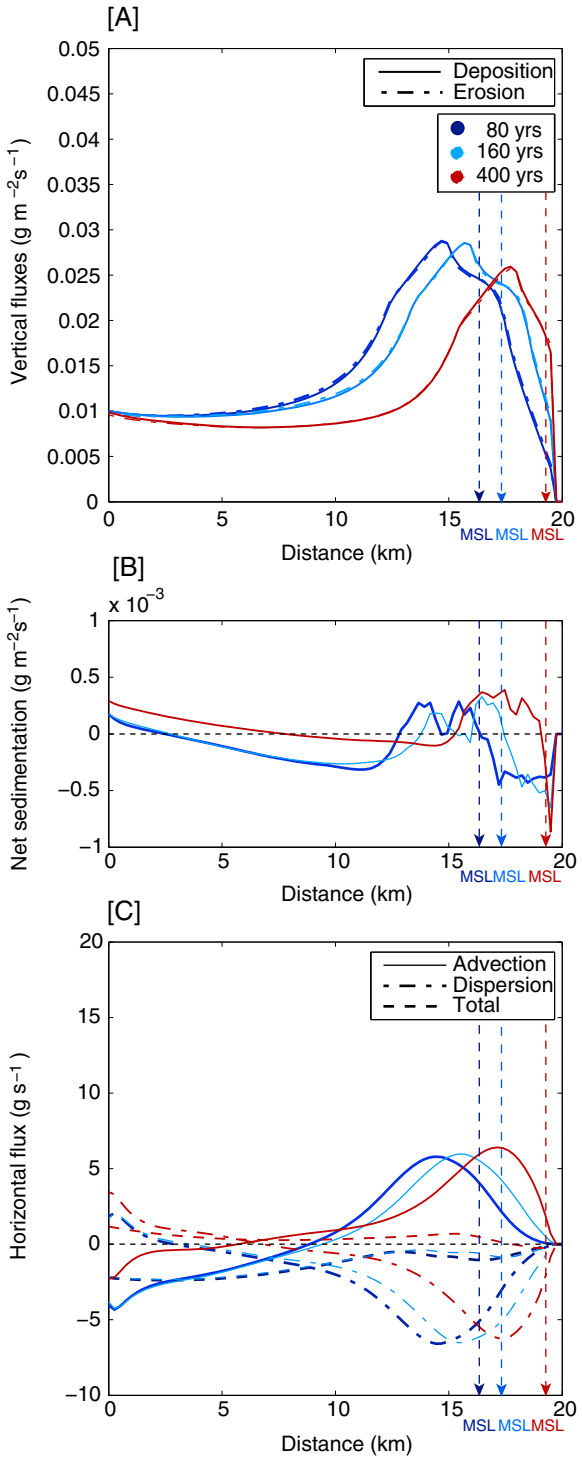

Figure 8. (Simulation *E*3) Tide-averaged sediment fluxes over the developing flat of Figure 6 after 80 years (dark blue) and 160 years (light blue) and over the equilibrium state after 400 years of evolution (dark red). (a) Deposition and erosion fluxes. (b) Net sedimentation. (c) Horizontal advection and dispersion fluxes. Landward is defined positive.

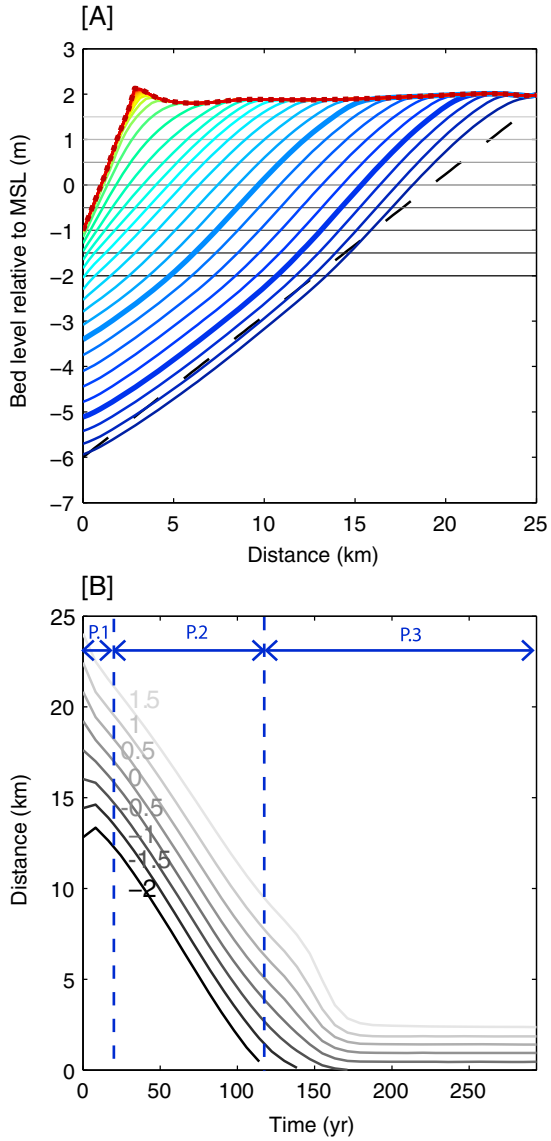

Figure 9. (a) Evolution from an initial bathymetry (from dashed black, via solid colored, to dotted red), under influence of tides and wind waves and $c_0 = 0.3$ kg m^{-3} (simulation *E*4) . The total time span is 280 years, with plotting time steps of 8 years. The gray horizontal lines refer to the bed levels of the lines in Figure 9b. (b) Distance toward the open boundary against time for different bed levels in the intertidal zone. Straight lines indicate a constant celerity. Parallel lines indicate an uniform celerity. Convergence or divergence of the lines indicate shape changes. At a relative short time scale, the flat evolves into a prograding system in which the shape and progradation speed is largely maintained (phase 2).

The tide-averaged dispersion flux is seaward over almost the entire intertidal flat, indicating that the real-time concentration is (generally) maximal close to the tidal front (i.e., at every moment in time the concentration gradient drives a seaward dispersion flux). The tide-averaged advection flux, on the other hand, is landward over the intertidal area but seaward on the lower (subtidal) flat. The net transport is seaward during the period of long-term retreat, indicating a predominance of dispersion processes on the intertidal flat. In the stationary equilibrium state, a net horizontal sediment transport remains over every tidal cycle. Over multiple tidal cycles the net transport balances out, so that the bed level remains steady in the long run.

2.3.4. Tides and Wind Waves—Progradation

For a sediment concentration at the boundary of 0.3 kg m^{-3}, a state of steady progradation develops within a few decades, see Figure 9. The action of wind waves results in local maxima in the tide-averaged gross erosion and deposition fluxes (and hence in the concentration) on the intertidal flat, which shift seaward as the flat progrades (Figure 10a). The maximum concentration is, however, found at the model boundary. In Figure 10b

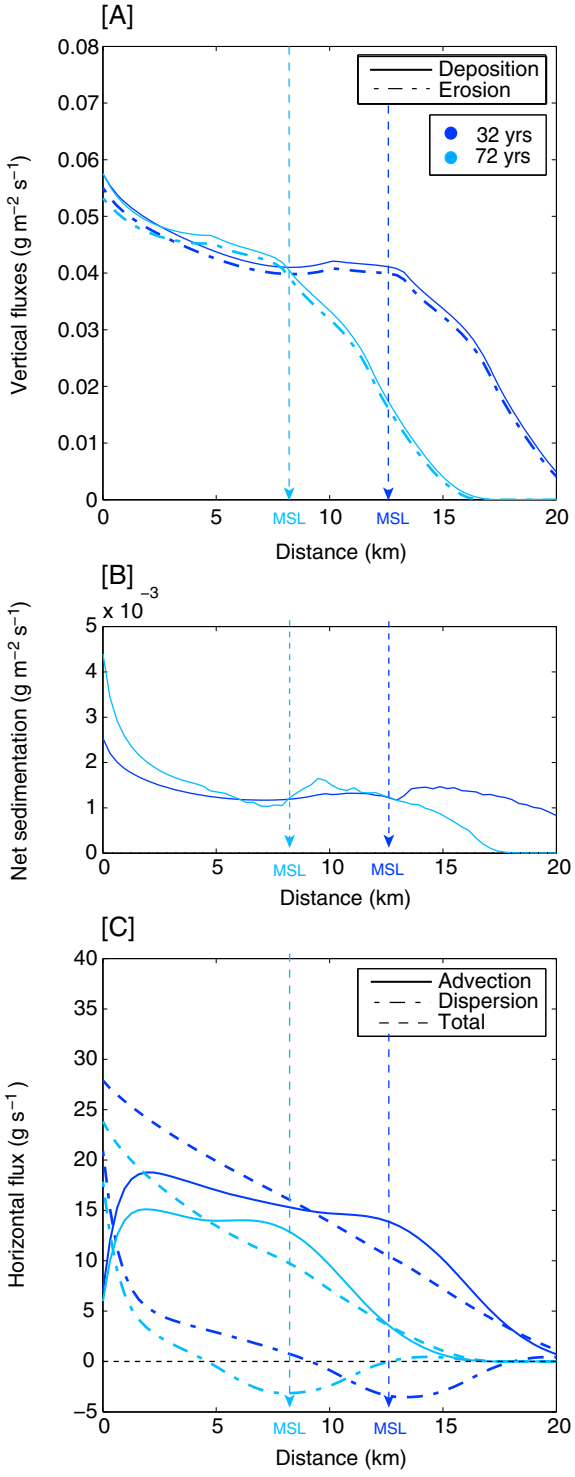

Figure 10. Tide-averaged sediment fluxes over the developing flat of Figure 9 after 32 years (dark blue) and 72 years (light blue) of evolution (i.e., on the thick lines with corresponding color in Figure 9) (simulation *E*4). (a) Deposition and erosion fluxes. (b) Net sedimentation. (c) Horizontal advection and dispersion fluxes. Landward is defined positive.

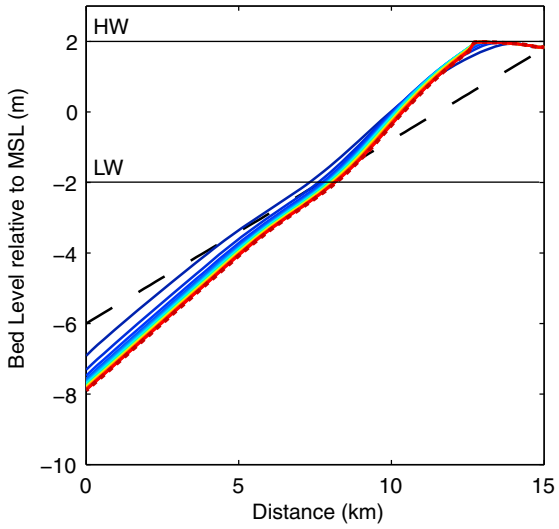

Figure 11. Evolution from an initial bathymetry (from the dashed black line, via the solid colored lines, to the dotted red line) in case of tides and waves, a suspended sediment concentration at the boundary of $5 \cdot 10^{-4}$ kg m^{-3}, and a dispersion coefficient of $K = 1$ m^2 s^{-1} (simulation *E5*). Time steps between two successive lines is 40 years, and the total time span is 840 years.

we see once more that the sedimentation rates in the prograding state are small compared with the gross deposition and erosion fluxes, but the differences are persistent (i.e., do not decrease in time). The horizontal sediment transport is mostly dominated by advection, which induces a landward transport (Figure 10c). Dispersion gives a negative (seaward) contribution over a large part of the intertidal flat.

2.3.5. Variation of the Dispersion Coefficient

To test the sensitivity of the results to the dispersion coefficient, the experiments were repeated with $K = 1$ m^2 s^{-1}. Only a little sensitivity to such a variation was found for high boundary concentrations (i.e., boundary concentrations that result in prograding profiles for $K = 100$ m^2 s^{-1}). This will be demonstrated and further discussed in section 3.3.2.

For lower boundary concentrations (that result in retreat for $K = 100$ m^2 s^{-1}), the state of the flat (progradation or retreat) was found to depend critically on the dispersion coefficient. For a concentration of 0.05 kg m^{-3} and a dispersion coefficient of $K = 1$ m^2 s^{-1}, the dispersion flux is negligible. Under influence of a net landward advection flux, a prograding state is established (opposed to the retreating state in Figure 6).

In order to determine the conditions for which a state of long-term retreat is established for $K = 1$ m^2 s^{-1}, the boundary concentration was lowered systematically. For a concentration of $C_0 = 5 \cdot 10^{-3}$ kg m^{-3}, a prograding state is established with a progradation speed of 2 m yr^{-1}. For $C_0 = 5 \cdot 10^{-4}$ kg m^{-3}, a retreating state was found for the first time, see Figure 11. Note that the relative difference between the gross erosion and deposition flux is very small (they are even indistinguishable in Figure 12a). Net sedimentation rates and a net seaward transport, however, remain (Figures 12c and 12d); in the very long run this intertidal flat is found to be erosive. Note furthermore that the role of the dispersion flux in the horizontal transport over the intertidal area is significant (Figure 12c), despite the low dispersion coefficient. On the subtidal flat, where the real-time concentration gradients are smaller, the transport is totally determined by (net seaward) advection.

2.4. Discussion

2.4.1. Horizontal Migration

Our results show that an equilibrium state is generally not (directly) reached. A stationary state only develops when waves are absent and the sediment concentration is zero at the boundary, in which case the shear stresses fall under the critical value for erosion. Such a stationary state for $C_0 = 0$ kg m^{-3} was also found by *Pritchard et al.* [2002]. In the other cases, a state of long-term progradation or retreat develops, depending on the combination of sediment supply and wave climate. The steady progradation obtained for a symmetric tide at the boundary and in the absence of wind waves is in agreement with the findings of *Pritchard et al.* [2002], *Waeles et al.* [2004], and *Le Hir et al.* [2007]. The horizontal migration of intertidal flats in the presence of wind

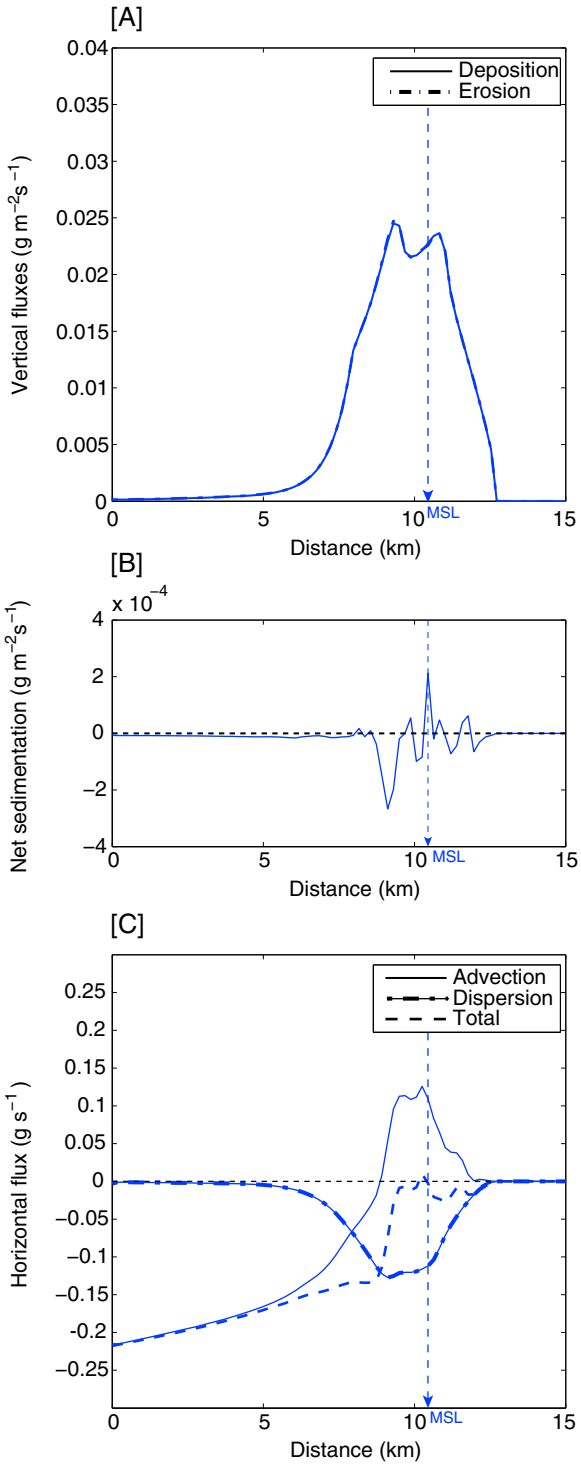

Figure 12. Tide-averaged sediment fluxes over the developing flat of Figure 11 after 840 years of evolution (simulation *E5*). (a) Gross deposition and erosion fluxes (these are hardly distinguishable in this plot). (b) Net sedimentation. (c) Horizontal advection and dispersion fluxes. Landward is defined positive.

waves has been produced before by *Mariotti and Fagherazzi* [2010] and *Tambroni and Seminara* [2012], while *Waeles et al.* [2004] noted that it depends on the typical wave regime whether a flat migrates horizontally or reaches a stationary equilibrium state. The dependency of the state (progradation or retreat) on the sediment supply is in accordance with the studies by *Mariotti and Fagherazzi* [2010] and *Tambroni and Seminara* [2012], which both discuss the importance of the amount of sediment supply in combination with the rate of sea level rise.

To understand the long-term evolution of intertidal flats and the reason why they do not (directly) approach a stationary equilibrium state (on the typical time scale at which the profile shape can adjust), we specify and distinguish the mechanisms which work in favor of such an equilibrium state from those working against it. For the explanation that follows, we first consider an initially accretive intertidal system with a constant sediment concentration at the seaward boundary. This implies that there is a net inflow of sediment and the elevation of the flat is increasing in time. Because the sediment concentration at the boundary is assumed to be constant, an equilibrium state could be approached mainly via an increase of the (tide-averaged) erosion over the intertidal flat, which would reduce the gradient in the seaward increasing concentration and the net inflow (via both advection and dispersion) of sediment. Hence, the question is whether an increase of the elevation of the flat leads to an increase (favoring equilibrium) or a decrease (resisting equilibrium) of the bed shear stresses on the flat. We will analyze this "morphodynamic feedback" for (1) tidal currents only and (2) tidal currents plus wind waves.

Furthermore, in order to understand the stable profile shape of prograding and retreating tidal flats, it is necessary to distinguish different sections of the intertidal area and to consider (1) for each section the "local morphodynamic feedback" (i.e., the effect of a local bed level change on the local imbalance) and (2) the morphodynamic feedbacks between the different sections (i.e., the feedback between a local bed level change and the surrounding tidal flat). In our analyses we assume that local imbalances between the deposition an erosion fluxes are affected (i.e., diminished or intensified) by the local bed level mainly via the erosion flux. This implies that the effect of a bed level change on the deposition flux is assumed to be relatively small. Note that the suspended sediment concentration (to which the deposition flux is linearly related via w_s) is determined by the space- and time-integrated deposition and erosion fluxes. Due to settling lag and scour lag effects, the local deposition flux depends on the erosion and deposition rates on the surrounding tidal flat and is therefore assumed to be less controlled by the local bed level than the local erosion flux.

2.4.2. Underlying Feedbacks—Tides Only

First, consider the situation without wind waves. The cross-shore tidal current velocity on the flat at a certain location and time can be approximated by [*Friedrichs and Aubrey*, 1996]

$$u(x) = \frac{1}{\beta}\frac{\mathrm{d}\zeta}{\mathrm{d}t}, \tag{21}$$

where β is the average bed slope from position x toward the position of the tidal front and $\zeta(t)$ the water level (in this derivation assumed to be homogeneous, i.e., uniform over the width of the tidal flat).

For a high concentration at the model boundary, net sedimentation will in first instance be most pronounced on the subtidal and lower intertidal flat, closest to the model boundary (note that the higher flat is too far away to receive sediment directly from the model boundary). On these sections, maximum currents are found during the maximum rate of water level variation and can be approximated by [*Friedrichs and Aubrey*, 1996; *Le Hir et al.*, 2000]

$$u(x) = \frac{\pi R}{\beta T_{\mathrm{tide}}}, \tag{22}$$

where β is now the average bed slope from position x toward the tidal front at mean sea level, T_{tide}, the tidal period, and R the tidal range. An increase in the bed level on the subtidal and lower flat would decrease the slope toward the tidal front over the whole period in which the bed is submerged, including the period of maximum tidal current. This would increase the tidal flow velocities, shear stresses, and the gross erosion flux over the period in which a section is underwater. This indicates a negative (stabilizing) feedback between the local bed level and the hydrodynamic forces: the erosion and deposition fluxes approach a local balance. Due to this negative feedback mechanism, the slopes on the lower tidal flat stabilize within the first decades of the evolution (see Figures 4, 6, and 9), although an exact balance on the lower flat cannot completely be reached

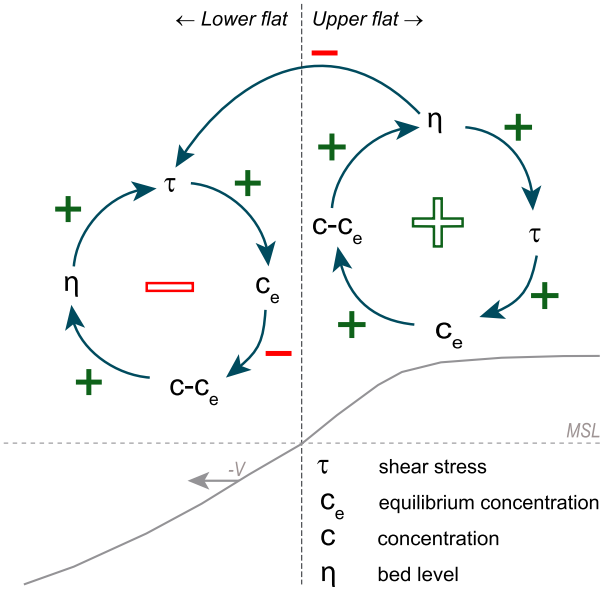

Figure 13. Feedback loops on a "tide controlled" flat. The arrows with positive and negative signs indicate positive and negative influences inbetween the parameters, respectively. An uneven number of negative influences within a loop results in a balancing feedback loop, whereas an even number of negative influences within a loop results in a reinforcing feedback loop. The bed level on the lower flat is controlled by a balancing feedback loop, i.e., if the deposition flux is initially larger than the erosion flux, i.e., $c - c_e > 0$, net sedimentation occurs and the bed level rises, resulting in locally larger tidal flow velocities and shear stresses, which diminish the initial imbalance. The bed level on the higher flat is controlled by a reinforcing feedback loop; an initial imbalance is amplified, because a rise (decay) in the bed level results in smaller (larger) tidal flow velocities and smaller (larger) shear stresses on the bed. At the same time, a rising upper flat reduces the tidal flow and shear stresses on the lower flat (indicated by the arrow with negative sign inbetween the loops), resulting in a migration of the whole flat.

before the upper intertidal flat is in balance (because the shear stresses are influenced by the upper intertidal flat morphology). At the same time, the increased erosion rates on the lower flat result in an increase in the sediment supply toward the higher sections.

As stated above, a rise in the bed level decreases the slope toward the tidal front over the whole period in which a location is submerged. This effect locally increases the shear stresses. However, on the higher sections of the intertidal area, an additional effect dominates the local morphodynamic feedback: Above msl, the time derivative of the water elevation (factor $\frac{d\zeta}{dt}$ in equation (21)), during the period in which a section is underwater, decreases with increasing elevation (with the most rapid decrease on the highest part of the tidal flat, assuming a sinusoidal water level variation in time). On the higher flat, an ascending bed level therefore leads to the exclusion of a period of maximum erosion rates. Hence, a rise in the bed level on this section is expected to cause a decrease in the erosion rates during the period in which a section is underwater. This implies that, once the supply toward the upper flat is abundant (and remains constant), there is no mechanism to increase the local erosion rates. As a result, sediment will accumulate on the upper part of the intertidal profile.

Different sections of the profile do not, however, evolve independently of each other: sedimentation on the upper intertidal flat increases the slopes from the lower flat toward the top of the flat (i.e., increase β in equations (21) and (22)) and hence decreases the tidal shear stresses on the lower sections: sedimentation on the upper flat will induce further seaward sedimentation. Because the local feedback on the lower flat favors local equilibrium, the slopes over the lower flat are continuously restored while the upper flat accretes. In this way, the flat shifts horizontally while the cross-shore shape, concentration gradients and sediment transport over the flat are conserved: a stationary balance cannot be established. Figure 13 outlines this concept.

Conversely, a state of long-term retreat, in which the flat retreats landward while the cross-shore shape is maintained, is to be expected in case of an erosive upper flat in combination with a "stable" lower flat: erosion on the upper intertidal flat would increase the tidal current velocities, bed shear stresses, and erosion rates on the lower sections and therefore induce a state of long-term retreat (i.e., the opposite of the situation in the foregoing paragraph). We could, however, not find such a state in case of tides only. The tidal flow velocities

and shear stresses generally decrease toward the shore, which favors a net landward sediment transport (see section 2.4.4).

2.4.3. Underlying Feedbacks—Tides and Wind Waves

Now we consider the situation in which wind waves are present. Because the lower elevations are generally dominated by tidal currents, the lower (sub) tidal flat is assumed to be stable (i.e., dominated by a negative feedback between the tide-induced erosion and the bed elevation, see above). For the part which is dominated by wind waves, the dependency of the erosion rates on the bed level is less straightforward.

Fagherazzi et al. [2006] and *De Swart and Zimmerman* [2009] explained the bimodal character of wave-dominated intertidal flats by considering the dependency of the wave-induced bed shear stress on the water depth. These studies consider the effect of locally generated wind waves on a platform with uniform (homogenous) water depth. The shear stress on the bed was found to be limited for both deep platforms (where the bottom is too deep to be affected by the waves) and shallow platforms (where the wave height is limited due to dissipation), and maximum for platforms with an intermediate water depth [*Fagherazzi et al.*, 2006]. For a tidal flat (with a tidal water level variation), this implies that the wave impact is limited to the subtidal elevations (where the water depths are mainly larger than the depth at which the maximum wave erosion occurs) and to the uppermost section of the intertidal range (where depths are mainly smaller than the one at which the maximum wave erosion occurs). Maximum erosion rates can be expected for intermediate elevations. This suggests that a stable interval exists from the elevation where waves start to dominate toward the elevation at which the maximum in wave erosion occurs, while an unstable interval could be expected for the higher part of the tidal range (after the location where the maximum in wave erosion occurs). This would result in a vertically migrating bed on the upper section; the bed accretes or erodes until a stable level is reached.

The situation is different, however, for a sloping bed and waves that approach the shore from deeper water. Our results indicate that in this situation maximum wave shear stresses occur close to the tidal front, i.e., in very shallow waters (see Figure 7). The height of the peaks is found to be more or less homogeneous over most of the intertidal flat. While the height of the peaks is roughly uniform, the time period over which maximum wave shear stresses occur is largest at high and low water tidal slacks, i.e., at locations where the water depths remain low for a long time, see *Waeles et al.* [2004]. On the lower flat, net sedimentation (net erosion) then decreases (increases) the time period of maximum wave shear stresses, which decreases (increases) the gross erosion flux and favors further sedimentation. Hence, an unstable section is to be expected on the lower intertidal flat, but only if wave-induced shear stresses locally dominate over the tide-induced shear stresses. On the higher tidal flat, net sedimentation (erosion) increases (decreases) the period of maximum wave shear stresses, so that this section is expected to be of a stable type.

The states of steady progradation and retreat for the combination of cross-shore tidal currents and wind waves can be understood by considering an additional wave-induced feedback mechanism: net accretion (erosion) of the lower flat results in more (less) wave dissipation and hence in smaller (larger) wave erosion rates on the higher flat. This implies that in case of a "wave-dominated" upper intertidal flat, the upper section cannot reach an exact balance before the lower intertidal flat is stable (because the wave-induced shear stresses are influenced by the seaward morphology). The lower (tide-dominated) intertidal flat, on the other hand, cannot reach a balance before the upper intertidal flat is stable (because the tide-induced shear stresses are influenced by the landward morphology, see section 2.4.2). Because net accretion (erosion) induces further accretion (erosion), a stationary equilibrium state cannot exist and the flat progrades or retreats horizontally (see Figure 14 for an outline of this concept).

2.4.4. Progradation or Retreat?

Once a stable profile shape is established, the long-term trend can be determined from the direction of the net sediment transport (which is maintained during the stage of steady migration, under the assumption of a constant boundary concentration). Let us now consider the mechanisms that drive these horizontal fluxes.

The tidal flow velocities generally decrease toward the shore. In the absence of wind waves, this determines the real-time concentration gradients. The real-time dispersion flux, as well as its time integral, is therefore landward. Decreasing tidal flow velocities and sediment concentrations toward the shore, in combination with settling and scour lag effects, also favor a net landward advection flux [*Van Straaten and Kuenen*, 1958]. The dominance of the landward advection flux (over the seaward advection flux during ebb) is further enhanced

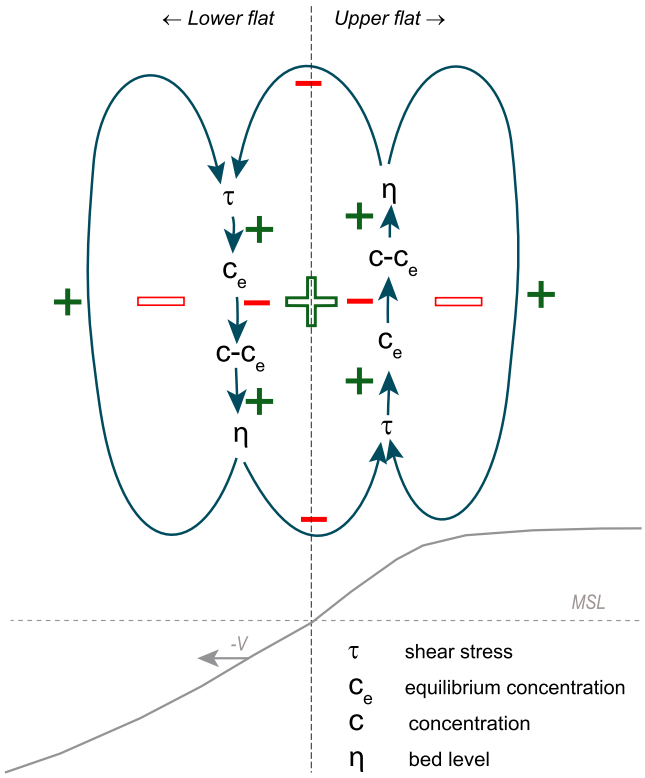

Figure 14. Feedback loops on a flat under influence of both cross-shore tidal currents and wind waves. The lower flat, dominated by tidal currents, is controlled by a stabilizing feedback loop, similar as in Figure 13. On the upper flat, net sedimentation (net erosion) increases (decreases) the time period of maximum wave shear stress and increases (decreases) the local gross erosion flux, which diminishes an initial imbalance. Hence, this section is also of a stabilizing type. The system is, however, unstable due to an additional reinforcing loop (indicated with a big plus sign in its center); net sedimentation on the lower flat will increase the wave dissipation and reduce the (wave-induced) shear stress on the higher flat. If the upper tidal flat was in an equilibrium state before, net sedimentation on the lower flat will result in net sedimentation on the higher flat. This, in turn results in a decrease in the tidal currents and tide-induced erosion rates on the lower flat and leads to a state of steady migration.

by a larger settling lag in deep water than in shallow water. Note that the sediment that is eroded on the lower flat, typically in larger water depths, stays in the water column for a longer time than sediment that is eroded on the (upper) intertidal flat. Hence, it travels longer horizontal distances before it settles again. Also, see the discussion on the effects of settling and scour lag provided by *Pritchard and Hogg* [2003].

In the presence of wind waves, on the other hand, maximum shear stresses and erosion rates occur on the intertidal flat. Because at each moment in time the maximum shear stresses occur close to the tidal front (where water depths are small, see Figure 7), a real-time concentration gradient is generated, which effectively drives a seaward dispersion flux of the eroded sediment (see Figure 7 for the real-time and Figures 8 and 10 for the tide-averaged wave-induced dispersion flux). The wave-induced concentration peaks on the intertidal flat will also enhance the advection flux during ebb and can alter the direction of the net advection flux. However, because the peaks occur in very shallow water, the sediment settles fast again after erosion (i.e., the depth-induced tidal asymmetry is still in favor of a net landward advection flux). Note that our results indicate a generally landward advection flux over the intertidal area, even in the presence of wind waves and concentration peaks on the intertidal flat (Figures 8, 10, and 12). States of steady retreat are then associated with a dominant seaward dispersion flux over the intertidal flat (Figures 8 and 12). In situations in which the tidal asymmetry is less pronounced in favor of flood, however, a net seaward advection flux would be feasible and the dispersion flux could be less relevant.

In the next section we will further investigate the influence of the sediment concentration at the boundary on the state (prograding or retreating) and shape of the profile.

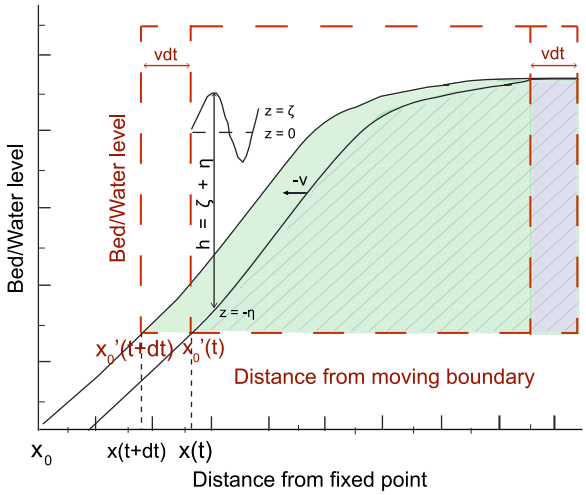

Figure 15. A stable bathymetry inside the Lagrangian reference frame for a prograding flat, indicated by the colored accentuated area at time t and by the green area at time $t + \mathrm{d}t$. $\zeta(x', t)$ is the water level, $\eta(x')$ is the bed level, and $h(x', t)$ is the water depth. Note that a negative velocity is assigned to seaward progradation.

3. Lagrangian Framework

3.1. Model Description

For deriving the stable profile shapes and velocities of migrating intertidal flats as a function of hydrodynamic forcing and sediment supply, we found that it is convenient to express the model in a Lagrangian reference frame, so that the boundary conditions specify one single steady state (described by a steady profile shape and migration velocity). This implies that the boundary conditions do not represent the conditions in a tidal channel any more but at a certain location (bed level) moving along with the prograding flat. Note that this approach is motivated by the observation that the concentration field shifts with the migration of the flat (section 2), so that the concentration remains constant for a given bed level. Note furthermore that the proposed method is incorporated in a purely morphodynamic model and does not require any preassumptions on the equilibrium profile shapes (consider *Wolinsky* [2009] for a discussion about morphokinematic models of shoreline migration).

We apply the following strategy to make the translation into the Lagrangian reference frame: we assign the boundary conditions (tidal range, wave climate, and sediment concentration) to an arbitrary bed level somewhere below the intertidal area. Defining the bed level at the boundary implies that the net sedimentation in the first grid cell is assumed to be completely captured by a horizontal movement of the coastline. The net sedimentation defines a migration velocity, which in turn defines a Lagrangian reference frame with spatial coordinate $x' = x + v \cdot t$ (see Figure 15). The equations for the hydrodynamics, sediment transport, and bed level changes are reformulated in this reference frame.

The conservation equations of (water) mass, momentum, and sediment in the Lagrangian reference frame contain an extra term, which couples the time derivatives in the stationary frame to the time derivatives in the moving system. This term is, however, always followed by a flow-advection term. Since the flow velocities of the water (u, in the order of m s^{-1}) are naturally much larger than the progradation speed of the coastline (v, in the order of m yr^{-1}), the extra term can be neglected.

Equation (1) becomes

$$\frac{\partial h}{\partial t} + \frac{\partial h}{\partial x'}\frac{\partial x'}{\partial t} + \frac{\partial uh}{\partial x'} = \frac{\partial h}{\partial t} + (v+u)\frac{\partial h}{\partial x'} + h\frac{\partial u}{\partial x'} \approx \frac{\partial h}{\partial t} + \frac{\partial uh}{\partial x'} = 0. \tag{23}$$

Equation (2) becomes

$$\frac{\partial u}{\partial t} + \frac{\partial u}{\partial x'}\frac{\partial x'}{\partial t} + u\frac{\partial u}{\partial x'} = \frac{\partial u}{\partial t} + (v+u)\frac{\partial u}{\partial x'} \approx \frac{\partial u}{\partial t} + u\frac{\partial u}{\partial x'} = -g\frac{\partial \zeta}{\partial x} - \frac{\tau_{bc}}{\rho_w h}. \tag{24}$$

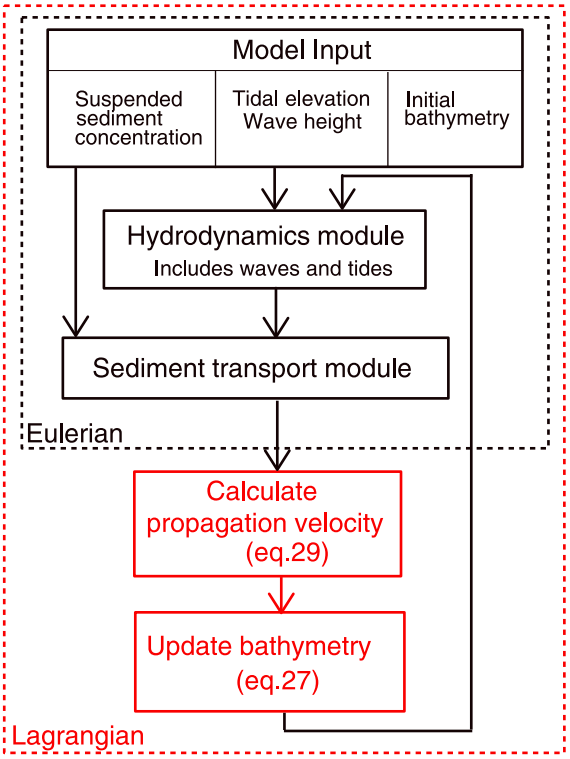

Figure 16. Schematic representation of the model in the Lagrangian framework, consisting of a conventional (Eulerian) part and an extra part in which the progradation velocity is calculated and used to update the bathymetry in the Lagrangian reference frame.

Equation (4) becomes

$$\frac{\partial ch}{\partial t}+\frac{\partial ch}{\partial x'}\frac{\partial x'}{\partial t}+\frac{\partial uch}{\partial x'}=\frac{\partial ch}{\partial t}+(v+u)\frac{\partial ch}{\partial x'}+ch\frac{\partial u}{\partial x'}\approx\frac{\partial ch}{\partial t}+\frac{\partial uch}{\partial x'}=\frac{\partial}{\partial x'}\left(Kh\frac{\partial c}{\partial x'}\right)+D-E. \tag{25}$$

In the Lagrangian reference frame, we can thus use the conventional conservation equations for mass, momentum, and sediment (equations (1), (2), and (4)). The only equation that significantly changes is the equation for the evolution of the bathymetry. In a moving reference frame, the time derivative of the bathymetry reads

$$\frac{\mathrm{d}\eta}{\mathrm{d}t}=\frac{\partial\eta}{\partial t}+\frac{\partial\eta}{\partial x'}\frac{\partial x'}{\partial t}. \tag{26}$$

Using $\frac{\partial\eta}{\partial t}=\frac{1}{\rho_{\mathrm{dry}}}(D-E)$ and $\frac{\partial x'}{\partial t}=v$, the horizontal migration velocity of the coastline, we find

$$\frac{\mathrm{d}\eta}{\mathrm{d}t}=\frac{1}{\rho_{\mathrm{dry}}}(D-E)+v\frac{\partial\eta}{\partial x'} \tag{27}$$

The profile shape is stable if

$$\frac{1}{\rho_{\mathrm{dry}}}\left(\overline{D}-\overline{E}\right)+v\frac{\partial\overline{\eta}}{\partial x'}=0, \tag{28}$$

in which the bars indicate tidal averages. In this "Lagrangian balance," net sedimentation is balanced by the velocity term in such a way that the cross-shore shape is maintained while the profile migrates. This implies that the net sedimentation is linearly proportional to the local slope of the profile; the steeper the slope, the more sedimentation (per surface area) is required for the same horizontal progradation (indicated by a thicker green nonaccentuated layer in Figure 15). Note that accretion dominance corresponds with a negative (seaward) velocity of the coastline (assuming a normally positive bed level gradient), whereas erosion dominance corresponds with a positive (landward) velocity term (see equation (28)).

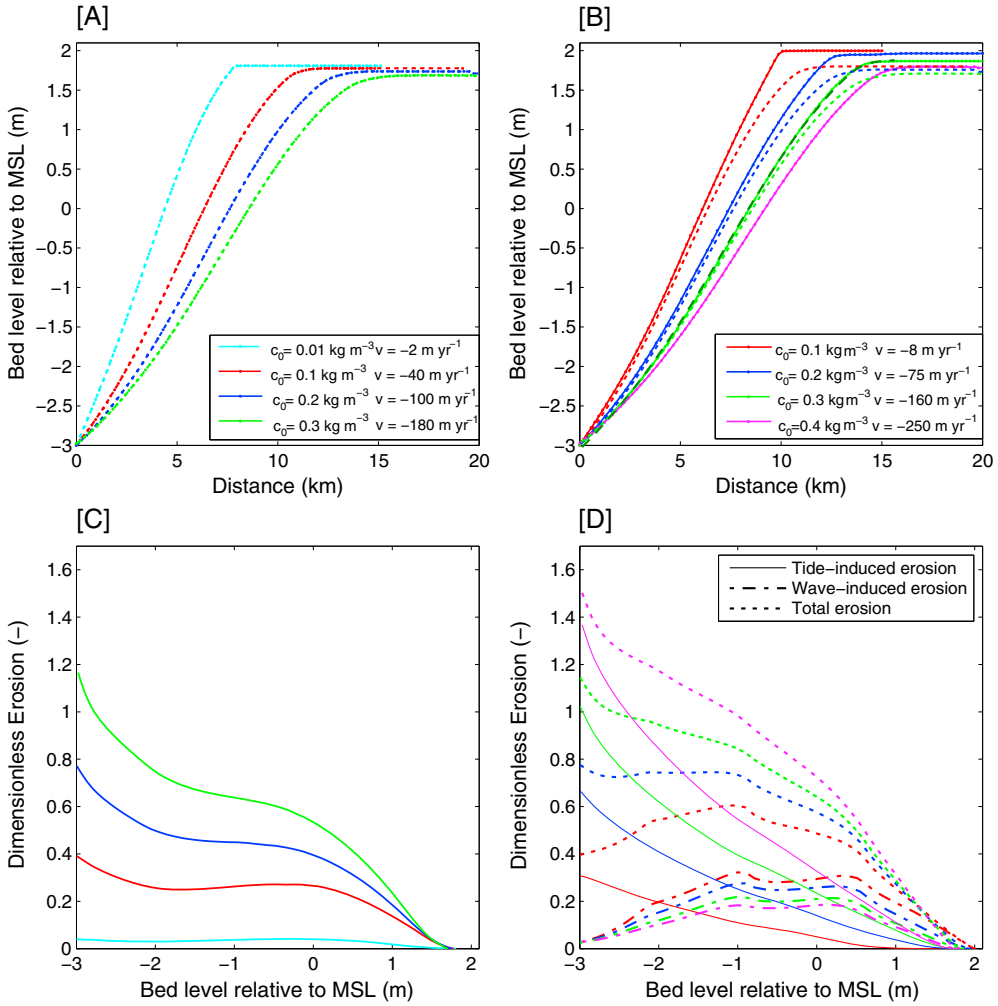

Figure 17. Lagrangian equilibrium profiles and progradation speeds for different concentrations of suspended sediment at the boundary. (a) Profiles for tides only (simulation *Lg*1–*Lg*4 in Table 2). (b) (Simulation *Lg*5–*Lg*8) Profiles for tides and wind waves (solid lines with markers). The dotted lines are copies from Figure 17a. The dark green dashed line is a profile obtained in an Eulerian framework for $c_0 = 0.3$ kg m^{-3}, i.e., a copy from Figure 9 after 80 years of evolution. Tide averages of the dimensionless erosion over the Lagrangian equilibrium profiles. (c) Tide averages of the dimensionless erosion over the profiles in Figure 17a. (d) Tide averages of the dimensionless erosion (total, tide-induced, and wave-induced) on the profiles in Figure 17b.

The migration velocity follows directly from the assumption of a constant bed level in the first grid cell and is defined by

$$v = -\frac{\left(\overline{D} - \overline{E}\right)}{\rho_{\text{dry}}\left(\frac{\partial \overline{\eta}}{\partial x'}\right)}\Big|_{x'=0} \tag{29}$$

Figure 16 shows a schematic representation of the model in the Lagrangian framework. The performance of the model in the Lagrangian framework has been tested by an elaborate comparison with the stable prograding profile shapes and migration velocities as obtained in the Eulerian framework. The results were found to be identical.

Since retreating profiles were not found in the Eulerian framework (due to the low hydrodynamic forces on the uppermost section of the intertidal area and the exclusion of cliff erosion), we apply the Lagrangian model only to derive prograding profiles (note that in principle the same method could be applied to derive retreating profiles as well, but it would require an additional formulation for cliff erosion).

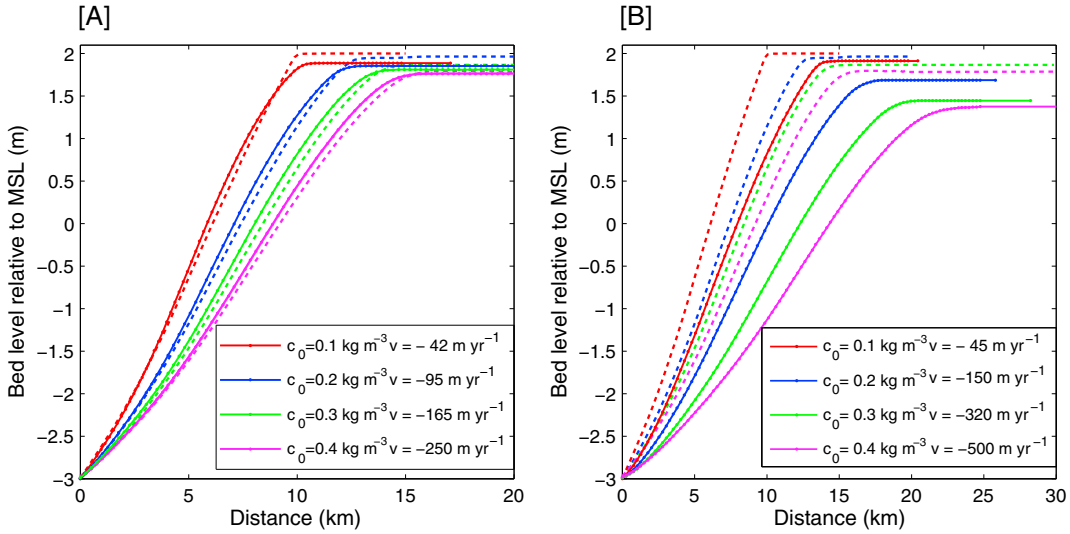

Figure 18. (a) Lagrangian equilibrium profiles and progradation speeds for $K = 1$ m^2 s^{-1}, under the influence of tides and wind waves (simulation *Lg*9–*Lg*12 in Table 2). The dotted lines are copies from Figure 17b, i.e., for $K = 100$ m^2 s^{-1}. (b) Lagrangian equilibrium profiles and progradation speeds for $w_s = 0.5 \cdot 10^{-3}$ m s^{-1}, under the influence of tides and wind waves (simulation *Lg*13–*Lg*16 in Table 2). The dotted lines are copies from Figure 17b, i.e., for $w_s = 0.2 \cdot 10^{-3}$ m s^{-1}.

3.2. Parameters and Boundary Conditions

The model parameters are chosen the same as in section 2.3 and summarized in Table 1. The shape and velocity of the obtained profiles are sensitive to the choice of the model parameters. Yet our qualitative results about the way in which the sediment supply influences the profile shape and the progradation velocity do not depend on the model parameters. The boundary conditions are assigned to an elevation of 1 m below lowest tide (i.e., msl −3 m), implying that the bed level in the first grid cell is fixed. A constant value is imposed for the sediment concentration at the seaward boundary. The water level variation and wave height at the seaward boundary are imposed in the same way as in section 2.3. Extra boundary conditions are required for the slopes in equations (27) and (29). The slope at the most landward and seaward grid cell is assumed to be zero and equal to that of its only neighbor, respectively. In order to fix the position of the landward boundary (i.e., an imaginary sea dike) in the Lagrangian reference frame, the length of the last (most landward) grid cell increases with the progradation of the coastline.

As in the previous section, the initial profile is a straight line. When starting from a gentle slope, the first grid cell is erosive and the bed in the model domain will initially rise via term 2 in equation (27), which steepens the profile slope. If a peak in the profile is formed seaward of the most landward cell, the area landward of the maximum bed elevation is omitted from the calculation and its bed level is taken equal to the peak value. Note that this section, which is shielded from the sediment supply and hydrodynamic forces, is not part of the migrating coastline (it will stay behind, while the part seaward of the top migrates, or it fills up by aeolian transport) and should be omitted because term 2 in equation (27) keeps acting also if erosion and deposition do not occur any longer.

3.3. Results

3.3.1. Lagrangian Equilibrium Profiles and Speeds

The effects of the boundary concentration on the steady progradation speed and profile shape of the intertidal flats are investigated for (1) tidal currents only and (2) tidal currents plus wind waves. The boundary concentration and wave settings for each simulation are summarized in Table 2.

The results show that an increase in the sediment concentration at the model boundary results in an increase in the progradation speed (i.e., in larger negative values) and gentler slopes (Figures 17a and 17b). Also, the presence of waves influences the speed and shape of the profile. For an identical sediment concentration at the boundary, the progradation speed is smaller and the upper profile is steeper if waves are present. The upward convexity of the profiles is thus determined by a combination of wind waves and sediment supply. For a sufficiently high boundary concentration, we find convex upward profiles, despite the presence of wind waves.

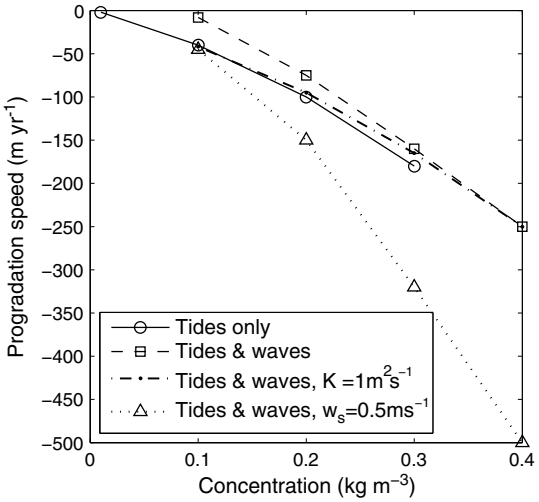

Figure 19. Lagrangian progradation speeds of the profiles in Figures 17 and 18 plotted against the sediment concentration at the model boundary (simulation *Lg*1–*Lg*16 in Table 2). $K = 100$ m^2 s^{-1} and $w_s = 0.2 \cdot 10^{-3}$ m s^{-1}, unless specified differently.

Figures 17c and 17d show that a high boundary concentration corresponds with large tide-induced erosion rates on the profiles. The wave-induced erosion, on the other hand, decreases with an increasing boundary concentration, but the deviation between the different simulations is relatively small (Figure 17d). Note that the values in these graphs have been made dimensionless by $\hat{E} = \frac{1}{m_e} E$ so that they are comparable with the dimensionless concentration $\hat{c} = \frac{w_s}{m_e} c$ (divide the values by 4 to obtain concentrations in kg m^{-3} and divide by 20 to obtain erosion rates in g m^{-2} s^{-2}). In Figure 17d, the wave- and tide-induced erosion has been calculated by $E_W = \max\left[m_e\left(\frac{\tau'_{bw}}{\tau_{cr}} - 1\right), 0\right]$ and $E_T = \max\left[m_e\left(\frac{\tau'_{bc}}{\tau_{cr}} - 1\right), 0\right]$, respectively, and their sum is slightly less than the total erosion rate.

3.3.2. Sensitivity to Model Parameters

The simulations in Figure 17b are repeated for a few different parameter settings (Figure 18). The profile slopes and shapes are not very sensitive to a variation of the dispersion coefficient K (see Figure 18a), but the progradation speeds are affected by a different value for K (Figure 19). A reduction in K results in an increase of the progradation speed (compare the squares with the dots in Figure 19). This effect is most pronounced for low boundary concentrations.

The results are also sensitive to a variation of the settling velocity. The slopes become gentler, and the progradation speeds increase with an increasing settling velocity (see Figures 18b and 19). Furthermore, the maximum elevation decreases with an increasing settling velocity (Figure 18b).

3.4. Discussion

Having discussed the feedback mechanisms underlying the long-term evolution of migrating flats in section 2, we here discuss the dependencies of the profile shape and progradation velocity on the wave climate and sediment supply.

In section 2 we showed that the local morphodynamic feedback is stabilizing on the lower flat, so that local balances between deposition and erosion are approached. The slopes (affecting tidal erosion) are adjusted via an increase or decrease of the bed levels, until the vertical fluxes are (approximately) in balance (section 2). Hence, a larger sediment concentration at the boundary results in the development of a gentler slope toward msl with larger tidal currents and tide-induced erosion rates (Figure 17), see also *Pritchard and Hogg* [2003]. If wind waves are added to the system (while maintaining the sediment concentration at the boundary), deposition and the total erosion, i.e., tide- plus wave-induced, approach a local equilibrium. Due to the contribution of wind waves to the total shear stresses, this equilibrium is found at smaller tidal flow velocities and steeper slopes than in the situation without waves (as can be seen from a comparison of the tide-induced erosion rates in Figures 17c and 17d).

Whereas the tidal erosion increases with an increasing boundary concentration (via the establishment of a local balance, see above), the wave erosion decreases with an increasing boundary concentration

(under assumption of a constant wave climate, see Figure 17d). This can be explained by the effect of the morphology on the wave dissipation: on a gentler slope, wave-induced bed friction dissipates more energy, so that the wave height is already reduced before the waves reach the elevation of maximum impact (note, however, that the amount of dissipation and the importance of this effect depends on the wave friction parameter).

Both the sediment concentration at the boundary and the presence of wind waves influence the progradation speed of the coastline (Figure 19). The progradation speed is determined by (1) the rate of sedimentation on the upper intertidal flat and (2) the sensitivity of the middle and lower intertidal flats to the accretion of the upper intertidal flat. A large sediment concentration at the boundary results in large tidal current velocities (see the explanation above) and hence a large tidal advection flux toward the upper intertidal flat. Subsequently, accretion of the upper intertidal flat feeds back efficiently onto the (tide-dominated) erosion rates over the other parts of the flat, inducing further seaward accretion. The effect of wind waves is twofold: (1) waves result in larger shear stresses (in combination with a larger seaward dispersion flux) and lower sedimentation rates on the upper intertidal flat and (2) they result in a smaller role for the tidal erosion on the middle and lower intertidal flat (due to the additional role of wind waves) and therefore decrease the sensitivity of the flat to the accretion on the upper part. This is translated into relatively steep slopes on the upper flat (compared with the situation in which waves are not present) and a lower progradation speed (under a constant sediment concentration at the boundary).

The Lagrangian equilibrium profiles and progradation velocities are, naturally, sensitive to variations in the parameter values (Figures 18 and 19). The seaward dispersion flux, driven by sharp concentration gradients at the tidal fronts (see section 2), is intensified by an increase in the dispersion coefficient, resulting in lower progradation speeds (Figure 19).

An increase in the settling velocity results in larger gross deposition fluxes at the boundary, which are balanced by larger gross erosion fluxes. Hence, the slopes get gentler (so that the tidal flow velocities increase) with an increasing boundary concentration (Figure 18b). The increase in the tide-induced erosion rates results in a larger sensitivity of the lower tidal flat to accretion on the upper part, which is reflected by larger migration velocities and a decrease in the maximum elevation of the migrating flat.

Despite these dependencies on model parameters, the tendency to evolve into states of steady migration, with a steady profile shape and migration speed, is not influenced by the considered variations of the parameter values.

4. The Evolution of the Yangtze Mudflats

The results of this modeling study suggest that an abundant sediment supply can result in a convex and prograding cross-shore profile of intertidal flats, despite the presence of eroding wind waves. This is in agreement with the observed convex and prograding profiles in the Yangtze Estuary [*Yang et al.*, 2011, Figure 1]. Also, the observed response of the Yangtze tidal flats to the reduction in sediment supply shows good similarity with the shift that might be expected from the model results.

The observed initial response to the reduction in sediment supply consists of erosion on the lower tidal flat, whereas accretion continues on the upper flat (Figure 1). This adjustment process steepens the slope of the profile. The observed response can be explained by the tendency of the intertidal system to approach a Lagrangian balance when forced with constant environmental conditions. If the flat used to be in a Lagrangian balance before, the lower flat would feel the reduction in the sediment availability directly. The supply toward the upper flat, on the other hand, would be highly determined by the erosion rates on the lower flat. The upper flat would therefore experience the change in boundary conditions only after an adjustment of the lower flat and be lagging relative to the response of the lower flat.

The steeper profile would subsequently result in smaller tidal flow velocities on the lower flat and smaller advection rates toward the upper intertidal flat. The model results suggest two different scenarios for the further response to the reduction in sediment availability:

1. The system evolves into a new Lagrangian balance, with a steeper slope over the lower flat. The net advection is still directed landward and large enough to overcome the wave-induced seaward dispersion flux, so that the system can prograde at a new (lower) progradation speed.
2. The net advection is seaward or not abundant to overcome the wave-induced erosion and dispersion flux. A state of long-term retreat is then to be expected. It is possible that the whole profile (including the

uppermost part) retreats landward. This is expected if the dissipation of wind waves over the flat and the associated decrease in the wave-induced forces toward the top of the profile is not significant or when cliff erosion plays a role. It is also possible that the uppermost part of the profile fills up, due to a decrease in the wave-induced force on the uppermost part of the profile, whereas the rest of the intertidal flat erodes. This would result in the development of a steep transition toward the top of the flat.

The change in shape of the Yangtze tidal flats has not yet resulted in net erosion at the higher flat (Figure 1). If the profile slope has already been stabilized (based on the typical time scales in the model simulations, this would happen within a few decades after the sediment availability in the Yangtze Estuary has been stabilized), a continuous progradation, albeit with a low progradation speed, would be expected from the model results. However, a further steepening of the lower intertidal flat would further decrease the advection of sediment toward the upper parts and increase the wave forces there (see section 3). In that case, a development toward a state of long-term retreat might occur.

5. Interpretations and Conclusions

This study confirms that intertidal systems that are controlled by cross-shore tidal currents, or a combination of cross-shore tidal currents and wind waves, converge to horizontally migrating "steady states," in which the cross-shore profile is maintained, as shown before by *Pritchard et al.* [2002]. The occurrence of these states is explained by the feedback mechanisms between the hydrodynamic forces and the intertidal flat morphology (section 2). While positive morphodynamic feedbacks drive the long-term horizontal migration of the flats, a negative feedback tends to stabilize the profile slope and shape within the first decades of evolution.

Because the concentration patterns shift with the migration of the flat, a constant concentration can be assigned as boundary condition of a 1-D cross-shore model expressed in a Lagrangian reference frame (i.e., which shifts with the migration velocity of the coastline). With such a model, the stable cross-sectional shape and progradation speed can be derived as a function of the sediment concentration at a fixed bed level. It has been shown that the cross-sectional shape does depend not only on the hydrodynamic forces but also on the sediment availability and is related to the progradation speed of the flat (section 3.3).

The influence of the upper intertidal flat morphology on the tide-induced shear stresses on the lower intertidal flat (explained in section 2) implies that the progradation speed of the flat can be influenced by engineering activities on the upper tidal flat. The construction of a sea dike around msl, for instance, would decrease the cross-shore tidal flow velocities on the lower sections and induce further seaward sedimentation. Also, artificial measures that favor deposition on the upper tidal flat, such as placing wave breakers or extra vegetation, would increase the progradation speed of the considered flats. It should, however, be mentioned that the inclusion of additional processes in the model could alter the dominant feedback mechanisms. In case of a large vegetation cover, biomorphodynamic feedbacks will play an important role [*Mariotti and Fagherazzi*, 2010], and the reflection of wind waves should be included for determining the effect of a sea dike around msl (as mentioned above).

In order to keep up with sea level rise, net sedimentation rates on the tidal flat should exceed the rate of sea level rise (SLR). Currently, the global average sea level rise is about 3 mm yr^{-1}. Assuming a gentle slope of 1:2000, this corresponds with a horizontal retreat of 6 m yr^{-1}. Considering the obtained migration speeds in Figures 17 and 18, the inclusion of SLR would only result in relative small adjustments of the results. For low progradation speeds, however, the state and shape of the flat can depend critically on SLR, as shown by the results of *Mariotti and Fagherazzi* [2010]. The flats that are considered in the study of *Mariotti and Fagherazzi* [2010] are subjected to more extreme wave conditions (indicated by the steeper slopes on the upper intertidal flat). In that case, net sedimentation rates are smaller due to a less significant role for the cross-shore tidal currents and the corresponding positive morphodynamic feedback mechanism. Hence, for those flats the state (prograding or retreating) depends more critically on SLR, for identical sediment concentrations at the boundary.

The kind of steady states that can be approached is characteristic for the underlying hydrodynamic forces and the morphodynamic feedback mechanisms. Our results only describe the behavior of wide flats that are dominated by cross-shore tidal currents and wind waves. This work can be seen as supplementary to the work of *Fagherazzi et al.* [2006], for instance, which describes the internal feedbacks on intertidal platforms that are controlled by locally generated wind waves only. These systems were found to converge to stationary

equilibrium states. In both cases, they are the local morphodynamic feedbacks that reveal the long-term evolution of intertidal flats.

Acknowledgments
We thank P. Le Hir and two anonymous reviewers for their constructive comments to improve the quality of the paper. We thank Q. Zhu for providing Figure 1b. This project is supported by the Netherlands Organization for Scientific Research (NWO) via the Joint Scientific Thematic Research Programme, project 842.00.007, Fate or future of intertidal flats in estuaries and tidal lagoons. All the data for producing the graphs and results for this paper are available upon request.

References

Ariathurai, C. R. (1974), A finite element model for sediment transport in estuaries, PhD thesis, Univ. of California, Berkeley, Calif.
Christoffersen, J. B., and I. G. Jonsson (1985), Bed friction and dissipation in a combined current and wave motion, *Ocean Eng.*, *12*(15), 387–423, doi:10.1016/0029-8018(85)90002-2.
Chu, A., Z. B. Wang, H. J. De Vriend, and M. J. F. Stive (2010), A process-based approach to sediment transport in the Yangtze Estuary, Conference on Coastal Engineering. Published by the Coastal Engineering Research Council, Shanghai, China. [Available at http://journals.tdl.org/icce/index.php/icce/article/view/1387/pdf_352, accessed date: 20-11-2015.]
De Swart, H. E., and J. T. F. Zimmerman (2009), Morphodynamics of tidal inlet systems, *Annu. Rev. Fluid Mech.*, *41*(1), 203–229, doi:10.1146/annurev.fluid.010908.165159.
Dyer, K. R. (1998), The typology of intertidal mudflats, in *Sedimentary Processes in the Intertidal Zone*, vol. 139, edited by K. B. Black, D. M. Paterson, and A. Cramp, pp. 11–24, Geol. Soc. Spec. Publ., London, doi:10.1144/GSL.SP.1998.139.01.02.
Eelkema, M., Z. B. Wang, A. Hibma, and M. J. F. Stive (2013), Morphological effects of the Eastern Scheldt storm surge barrier on the ebb-tidal delta, *Coast. Eng. J.*, *55*(3), 1350010, doi:10.1142/S0578563413500101.
Fagherazzi, S., L. Carniello, L. D'Alpaos, and A. Defina (2006), Critical bifurcation of shallow microtidal landforms in tidal flats and salt marshes, *Proc. Natl. Acad. Sci. U.S.A.*, *103*(22), 8337–8341, doi:10.1073/pnas.0508379103.
Fagherazzi, S., C. Palermo, M. C. Rulli, L. Carniello, and A. Defina (2007), Wind waves in shallow microtidal basins and the dynamic equilibrium of tidal flats, *J. Geophys. Res.*, *112*, F0204, doi:10.1029/2006JF000572.
Fischer, H. B. (1976), Mixing and dispersion in estuaries, *Annu. Rev. Fluid Mech.*, *8*, 107–133, doi:10.1146/annurev.fl.08.010176.000543.
Flemming, B. W. (2002), Geographic distribution of muddy coasts, in *Muddy Coasts of the World*, edited by T. Healy, Y. Wang, and J.-A. Healy, pp. 99–201, Elsevier, Amsterdam.
Fredsoe, J., and R. Deigaard (1992), *Advanced Series on Ocean Engineering*, vol. 3, World Scientific, Singapore.
Friedrichs, C. T. (2011), Tidal flat morphodynamics: A synthesis, in *Treatise on Estuarine and Coastal Science*, edited by E. Wolanski and D. McLusky, pp. 137–137, Academic Press, Waltham, Mass., doi:10.1016/B978-0-12-374711-2.00307-7.
Friedrichs, C. T., and D. G. Aubrey (1996), Uniform bottom shear stress and equilibrium hyposometry of intertidal flats, in *Mixing in Estuaries and Coastal Seas., Coastal Estuarine Ser.*, vol. 50, edited by C. Pattiaratchi, 405–429, AGU, Washington, D. C., doi:10.1029/CE050p0405.
Hu, K., P. Ding, Z. B. Wang, and S. Yang (2009), A 2D/3D hydrodynamic and sediment transport model for the Yangtze Estuary, China, *J. Mar. Syst.*, *77*, 114–136, doi:10.1016/j.jmarsys.2008.11.014.
Justesen, P. (1988), Turbulent wave boundary layers, PhD thesis, Techn. Univ. Denmark, Inst. of Hydrodyn. and Hydraul. Eng., ISVA, Denmark.
Geyer, W. R., and R. P. Signell (1992), A reassessment of the role of tidal dispersion in estuaries and bays, *Estuaries*, *15*(2), 97–108, doi:10.2307/1352684.
Kirby, R. (2000), Practical implications of tidal flat shape, *Cont. Shelf Res.*, *20*, 1061–1077, doi:10.1016/S0278-4343(00)00012-1.
Kirby, R. (2002), Distinguishing accretion from erosion-dominated muddy coasts, in *Muddy Coasts of the World*, edited by T. Healy, Y. Wang, and J.-A. Healy, pp. 61–81, Elsevier, Amsterdam.
Lee, S., and A. J. Mehta (1997), Problems in characterizing the dynamics of mud shore profiles, *J. Hydraul. Eng.*, *4*, 351–361, doi:10.1061/(ASCE)0733-9429(1997)123:4(351).
Le Hir, P., W. Roberts, O. Cazaillet, M. Christie, P. Bassoullet, and C. Bacher (2000), Characterization of intertidal flat hydrodynamics, *Cont. Shelf Res.*, *20*(12–13), 1433–1459, doi:10.1016/S0278-4343(00)00031-5.
Le Hir, P., Y. Monbet, and F. Orvain (2007), Sediment erodability in sediment transport modelling: Can we account for biota effects?, *Cont. Shelf Res.*, *27*, 1116–1142, doi:10.1016/j.csr.2005.11.016.
Lesser, G. R., J. A. Roelvink, J. A. T. M. van Kester, and G. S. Stelling, Development and validation of a three-dimensional morphological model, *Coast. Eng.*, *51*(8–9), 883–915, doi:10.1016/j.coastaleng.2004.07.014.
Liu, X. J., S. Gao, and Y. P. Wang (2011), Modeling profile shape evolution for accreting tidal flats composed of mud and sand: A case study of the central Jiangsu coast, China, *Cont. Shelf Res.*, *31*, 1750–1760, doi:10.1016/j.csr.2011.08.002.
Marani, M., A. D'Alpaos, S. Lanzoni, L. Carniello, and A. Rinaldo (2007), Biologically-controlled multiple equilibria of tidal landforms and the fate of the Venice lagoon, *Geophys. Res. Lett.*, *34*, L11402, doi:10.1029/2007GL030178.
Marani, M., A. D'Alpaos, S. Lanzoni, L. Carniello, and A. Rinaldo (2010), The importance of being coupled: Stable states and catastrophic shifts in tidal biomorphodynamics, *J. Geophys. Res.*, *115*, F04004, doi:10.1029/2009JF001600.
Mariotti, G., and S. Fagherazzi (2010), A numerical model for the coupled long-term evolution of salt marshes and tidal flats, *J. Geophys. Res.*, *115*, F01004, doi:10.1029/2009JF001326.
Mehta, A. J., R. Kirby, and S.-C. Lee (1996), *Some Observations on Mudshore Dynamics and Stability*, Coastal and Oceanographic Engineering Department, Univ. of Florida. Report No. UFL/COEL/MP-96/1 to U.S. Army Corps of Engineers.
Pritchard, D., and A. J. Hogg (2003), Cross-shore sediment transport and the equilibrium morphology of mudflats under tidal currents, *J. Geophys. Res.*, *108*(C10), 3313, doi:10.1029/2002JC001570.
Pritchard, D., A. J. Hogg, and W. Roberts (2002), Morphological modelling of intertidal mudflats: The role of cross-shore tidal currents, *Cont. Shelf Res.*, *22*, 1887–1895, doi:10.1016/S0278-4343(02)00044-4.
Roberts, W., P. Le Hir, and R. J. S. Whitehouse (2000), Investigation using simple mathematical models of the effect of tidal currents and waves on the profile shape of intertidal mudflats, *Cont. Shelf Res.*, *20*, 1079–1097, doi:10.1016/S0278-4343(00)00013-3.
Roelvink, J. A. (2006), Coastal morphodynamic evolution techniques, *Coastal Eng.*, *53*(2–3), 277–287, doi:10.1016/j.coastaleng.2005.10.015.
Shi, B. W., S. L. Yang, Y. P. Wang, T. K. Bouma, and Q. Zhu (2012), Relating accretion and erosion at an exposed tidal wetland to the bottom shear stress of combined current-wave action, *Geomorphology*, *138*, 380–389, doi:10.1016/j.geomorph.2011.10.004.
Soulsby, R. (1997), *Dynamics of Marine Sands. A Manual for Practical Applications*, Thomas Telford, London.
Soulsby, R. L., and S. Clarke (2005), *Bed Shear-Stresses Under Combined Waves and Currents on Smooth and Rough Beds*, Report TR137, HR Wallingford, Oxfordshire. [Available at http://books.hrwallingford.co.uk/acatalog/free_downloads/ TR137.pdf, accessed date: 20-11-2015.]
Stelling, G. S., and S. P. A. Duinmeijer (2003), A staggered conservative scheme for every Froude number in rapidly varied shallow water flows, *Int. J. Numer. Methods Fluids*, *43*(12), 1329–1354, doi:10.1002/fld.537.
Swart, D. (1976), Predictive equations regarding coastal transport, in *Proceeding of 15th Conference on Coastal Engineering*, pp. 1113–1132, ASCE, Honolulu, Hawaii., doi:10.9753/icce.v15.

Tambroni, N., and G. Seminara (2012), A one-dimensional eco-geomorphic model of marsh response to sea level rise: Wind effects, dynamics of the marsh border and equilibrium, *J. Geophys. Res.*, *117*, F03026, doi:10.1029/2012JF002363.

Ter Brake, M. C., and H. M. Schuttelaars (2010), Modeling equilibrium bed profiles of short tidal embayments, *Ocean Dyn.*, *60*, 183–204, doi:10.1007/s10236-009-0232-3.

van de Koppel, J., D. van der Wal, J. P. Bakker, and P. M. J. Herman (2005), Self-organization and vegetation collapse in salt marsh ecosystems, *Am. Nat.*, *165*(1), E1–E12, doi:10.1086/426602.

Van der Wegen, M. (2010), Modeling morphodynamic evolution in alluvial estuaries, PhD thesis, Delft Univ. of Technology and UNESCO-IHE Institute for Water Education, Netherlands.

van Prooijen, B. C., and Z. B. Wang (2013), A 1D model for tides waves and fine sediment in short tidal basins—Application to the Wadden Sea, *Ocean Dyn.*, *63*, 1233–1248, doi:10.1007/s10236-013-0648-7.

Van Rijn, L. C. (1993), *Principles of Sediment Transport in Rivers, Estuaries and Coastal Seas*, Aqua Publ., Amsterdam.

Van Straaten, L., and P. H. Kuenen (1958), Tidal action as a cause of clay accumulation, *J. Sediment. Res.*, *28*(4), 406–413, doi:10.1306/74D70826-2B21-11D7-8648000102C1865D.

Waeles, B., P. Le Hir, and R. S. Jacinto (2004), Modelisation morphodynamique cross-shore d'un estran vaseux, *C. R. Geosci.*, *336*, 1025–1033, doi:10.1016/j.crte.2004.03.011.

Winterwerp, J. C., and W. G. Van Kesteren (2004), *Introduction to the Physics of Cohesive Sediment Dynamics in the Marine Environment*, 56 pp., Developments in Sedimentology, Elsevier, Amsterdam.

Wolinsky, A. W. (2009), A unifying framework for shoreline migration: 1. Multiscale shoreline evolution on sedimentary coasts, *J. Geophys. Res.*, *114*, F01008, doi:10.1029/2007JF000855.

Yang, S. L., P. X. Ding, and S. L. Chen (2001), Changes in progradation rate of the tidal flats at the mouth of the Changjiang Yangtze River, China, *Geomorphology*, *38*, 167–180, doi:10.1016/S0169-555X(00)00079-9.

Yang, S. L., H. Li, T. J. Ysebaert, T. J. Bouma, W. X. Zhang, P. Li, M. Li, and P. X. Ding (2008), Spatial and temporal variations in sediment grain size in tidal wetlands, Yangtze Delta: On the role of physical and biotic controls, *Estuarine Coastal Shelf Sci.*, *77*, 657–671, doi:10.1016/j.ecss.2007.10.024.

Yang, S. L., J. D. Milliman, P. Li, and K. Xu (2011), 50,000 dams later: Erosion of the Yangtze River and its delta, *Global Planet. Change*, *75*(1–2), 14–20, doi:10.1016/j.gloplacha.2010.09.006.

Zimmerman, J. T. F. (1976), Mixing and flushing of tidal embayments in the Western Dutch Wadden Sea, Part II: Analysis of mixing processes, *Neth. J. Sea Res.*, *10*, 397–439, doi:10.1016/0077-7579(76)90013-2.